Eur. Phys. J. D **60**, 137–156 (2010)
DOI: 10.1140/epjd/e2010-00107-7

THE EUROPEAN PHYSICAL JOURNAL D

Regular Article

Ultrafast resonance energy transfer in bio-molecular systems

P.K. Verma and S.K. Pal[a]

Unit for Nano Science & Technology, Department of Chemical, Biological & Macromolecular Sciences, S.N. Bose National Centre for Basic Sciences, Block JD, Sector III, Salt Lake, 700098 Kolkata, India

Received 14 December 2009 / Received in final form 28 January 2010
Published online 26 April 2010 –

Abstract. In this article, we present our consistent efforts to explore the dynamical pathways of the migration of electronic radiation by using ultrafast (picosecond/femtosecond time scales) Förster resonance energy transfer (FRET) technique. The ultrafast non-radiative energy migration from an intrinsic donor fluorophore (Tryptophan, Trp214) present in domain IIA of a transporter protein human serum albumin (HSA) to various non-covalently/covalently attached organic/inorganic chromophores including photoporphyrin IX (PPIX), polyoxovanadate $[V_{15}As_6O_{42}(H_2O)]^{-6}$ clusters (denoted as V_{15}) and CdS quantum dots (QDs) has been explored. We have also used other covalently/non-covalently attached extrinsic fluorogenic donors (NPA, ANS) in order to exploit the dynamics of resonance energy migration of an enzyme α-chymotrypsin (CHT). The use of extrinsic donor instead of intrinsic Trp in CHT avoids ambiguity in the location of the donor molecule as seven tryptophans are present in the enzyme CHT. We have labeled CHT with ANS (1-anilinonaphthalene-8-sulfonate) and NPA (4-nitrophenyl anthranilate) and studied FRET. Labeling of DNA has also been done in the context that the DNA bases have very low quantum yield for fluorescence. We have also validated FRET model over nano-surface energy transfer technique (NSET) in the case of quantum clusters and applied the findings to other QDs. The use of QDs over organic fluorophore was justified by least photo-bleaching of QDs compared to organic fluorophore. Our studies may find relevance in the exploration of alternate pathway for ultrafast migration of electronic radiation through FRET to minimize the detrimental effect of UV radiation in living organism.

1 Introduction

Sunlight, which is essential for life on earth, contains significant amounts of harmful UV ($\lambda < 400$ nm) radiation. These solar UV photons constitute one of the most ubiquitous and potent environmental carcinogens. Many studies have demonstrated that ultraviolet (UV) radiation can damage proteins or cell membranes, and generate oxidative stress, it is generally accepted that its major deleterious effects are mediated by specific DNA lesions arising from the direct absorption of photons. These lesions have been reported to play an important role in the induction of the lethal, mutagenic, and tumorigenic effects of UV exposure [1]. Ultraviolet radiation poses, in this respect, a serious threat to the well-ordered sequence of hydrogen-bonded DNA base pairs [2–6]. Although all nucleic acid bases can exist in a variety of energetically close-lying tautomeric forms, only one tautomer of each species is present in the canonical base pairs of healthy DNA. Knowledge of the photophysical properties of nucleic acid bases is the key to understand radiation induced genetic damage.

UV light was experimentally demonstrated to cause DNA damage mostly by the formation of dimeric photoproducts between adjacent pyrimidine bases on the same strand [7]. DNA dimerization of pyrimidines induced by UV leads to the distortion of DNA structure, which may result in cytotoxicity, mutagenicity, and the induction of cell signaling pathways. Indeed, pyrimidine dimers can block DNA replication, cell division, and DNA transcription needed for the synthesis of messenger RNA, which is a crucial step for protein production and cell survival. These considerations explain why cells have evolved elaborate mechanisms to identify and repair damage before it blocks replication or causes a mutation. Cells would not endure long without such mechanisms. A process called photoreactivation uses DNA photolyase to directly reverse the formation of pyrimidine dimers that results from UV irradiation [8,9]. Photolyases are widespread in nature and, for example, have been reported in many bacteria, blue-green algae, fungi, higher plants and all major groups of vertebrates, with the possible exception of placental mammals. In photoreactivation, the enzyme DNA photolyase captures energy from light and uses it to break the covalent bond linking adjacent pyrimidines [9]. Photolyase is a monomeric protein that contains two chromophore/cofactors, flavin and folate (or deazaflavin). One chromophore (folate) is used for light absorption, and the other (flavin) for chemistry. This is supported by the absorptivities of the two chromophores: folate exhibits $\varepsilon = 25\,000\ \mathrm{M^{-1}\,cm^{-1}}$ vs. $\varepsilon = 5000\ \mathrm{M^{-1}\,cm^{-1}}$ for $FADH^-$.

[a] e-mail: skpal@bose.res.in

It has been shown that Förster resonance energy transfer (FRET) occurs via dipole-dipole coupling between folate and flavin [10].

Thus it is evident that ultrafast migration of electronic radiation (UV) in DNA is not only important for the protection of the genetic material from UV damage but also equally important for the recovery of the damage through a directed resonance energy transfer in biologically relevant chromophores. As photolysases are possibly absent in placental mammals it becomes extremely important to find an alternate path through FRET to minimize the effect in placental mammals. The ultrafast migration of electronic radiation is equally important in the light harvesting processes in important biological systems including photosynthesis. In biological systems, light harvesting uses the energy in photons to drive chemical reactions. In proteins, a series of chromophores are used to separate charges and avoid back reactions. The energy passes between chromophores through FRET. If the chromophores are close enough together typically within a few nanometres then they are coupled like two pendulums attached to the same beam: if one starts oscillating, it can set the other moving. This coupling depends not only on distance but also on the relative orientation of the two chromophores (donor and acceptor). Hence it becomes extremely important to study FRET in biological systems. Exploration of the scope of the ultrafast resonance energy transfer in various biologically relevant environments is the motive of the present studies.

In our studies we explored the resonance energy transfer from one of the fluorescent amino acids tryptophan (Trp214) in domain IIA of human serum albumin (HSA) as a donor to acceptors like photoporphyrin IX (PPIX) [11], molecular magnet [12] and quantum dots (QDs) [13] in FRET based systems. For the enzyme α-chymotrypsin (CHT), the choice of the tryptophan as donor is ruled out as there are seven of them present in CHT. The choice of probe like ANS (1-anilinonaphthalene-8-sulfonate) or NPA (4-nitrophenyl anthranilate) was made on the basis of the selection of a specific molecular site in case of CHT. NPA is known to bind at the catalytic center of CHT whereas ANS binds diagonally opposite in position to the catalytic center. For the investigation of FRET in DNA, natural DNA bases are not good choice because of their very low emission quantum yield. Here we will also discuss the labeling of the DNA with fluorescent species to make a complete FRET based system and establish the fact that the relative orientation of the transition dipoles of donor (D) and acceptor (A) plays an important role in the energy transfer when D and A are simultaneously bound in a confined geometry of a dodecamer DNA [14]. The use of organic fluorophores (dyes) in the FRET studies on biological macromolecules often suffer from unavoidable photo-bleaching of dyes. In this regard, QDs have an advantage over organic dyes in that they can be tailored to obtain the desired fluorescent properties: high quantum yield, high photostability, high extinction coefficient and narrow emission spectra but with a broad excitation band. While using QDs, it becomes equally important to establish the validation of FRET over nanosurface energy transfer technique (NSET) which comes from the damping of the donor fluorophore's oscillating dipole by the acceptor QDs through either electron hole pair (EHP) for semiconductor or free electrons for metal. In this respect we will discuss the validation of FRET over NSET in the case of quantum metal clusters and apply the finding to other systems like QDs.

2 Methodology

2.1 Förster resonance energy transfer (FRET) technique

FRET is an electrodynamic phenomenon involving the non-radiative transfer of the excited state energy from the donor dipole (D) to an acceptor dipole (A) in the ground state in a distance dependent manner (Fig. 1a). Since the energy transfer efficiency is distance dependent, it is also known as "spectroscopic ruler" [15]. FRET is very often used to measure the distance between two sites on a macromolecule. FRET has got wide uses in all fluorescence applications including medical diagnostics, DNA analysis, imaging, sensing, detection, therapy, and monitoring structural changes of biomolecules. Basically, FRET is of two types: (a) homo-molecular FRET and (b) hetero-molecular FRET. In the former case the same fluorophore acts both as energy donor and acceptor, while in the latter case two different molecules act as donor and acceptor.

Each donor-acceptor (D-A) pair participating in FRET is characterized by a distance known as Förster distance (R_0) i.e., the D-A separation at which energy transfer is 50% efficient. The R_0 value ranges typically from 20 to 60 Å. The rate of resonance energy transfer (k_T) from donor to an acceptor is given by,

$$k_T = \frac{1}{\tau_D}\left(\frac{R_0}{r}\right)^6 \tag{1}$$

where τ_D is the lifetime of the donor in the absence of acceptor and r is the donor to acceptor (D-A) distance. The rate of transfer of donor energy depends upon the extent of overlap of the emission spectrum of the donor with the absorption spectrum of the acceptor ($J(\lambda)$), the quantum yield of the donor (Q_D), the relative orientation of the donor and acceptor transition dipoles (κ^2) and the distance between the donor and acceptor molecules (r) (Fig. 1b). In order to estimate FRET efficiency of the donor and hence to determine distances between donor-acceptor pairs, the methodology described below is followed [16,17]. R_0 is given by,

$$R_0 = 0.211\left[\kappa^2 n^{-4} Q_D J(\lambda)\right]^{1/6} \quad \text{(in Å)} \tag{2}$$

where n is the refractive index of the medium, Q_D is the quantum yield of the donor and $J(\lambda)$ is the overlap integral. κ^2 is defined as,

$$\begin{aligned}\kappa^2 &= (\cos\theta_T - 3\cos\theta_D\cos\theta_A)^2 \\ &= (\sin\theta_D\sin\theta_A\cos\varphi - 2\cos\theta_D\cos\theta_A)^2\end{aligned} \tag{3}$$

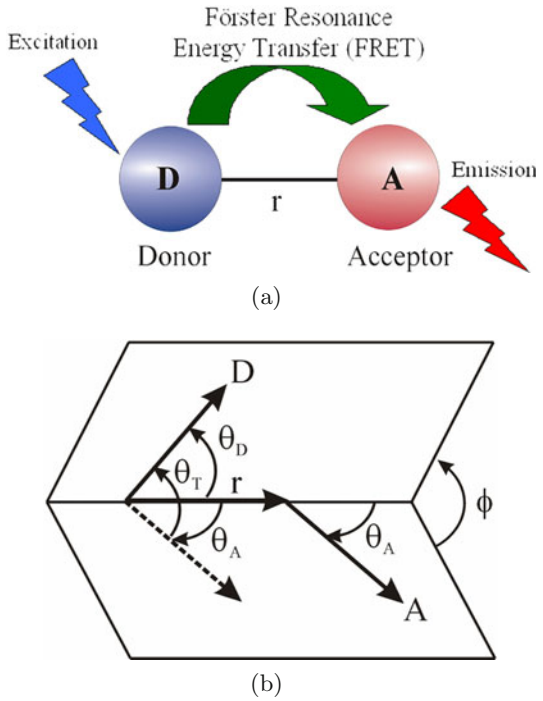

Fig. 1. (Color online) (a) Schematic illustration of the Förster resonance energy transfer (FRET) process. (b) Dependence of the orientation factor κ^2 on the directions of the emission and absorption dipoles of the donor and acceptor, respectively.

where θ_T is the angle between the emission transition dipole of the donor and the absorption transition dipole of the acceptor, θ_D and θ_A are the angles between these dipoles and the vector joining the donor and acceptor and φ is angle between the planes of the donor and acceptor (Fig. 1b). κ^2 value can vary from 0 to 4. For collinear and parallel transition dipoles, $\kappa^2 = 4$; for parallel dipoles, $\kappa^2 = 1$; and for perpendicularly oriented dipoles, $\kappa^2 = 0$. For donor and acceptors that randomize by rotational diffusion prior to energy transfer, the magnitude of κ^2 is assumed to be 2/3. However, in systems where there is a definite site of attachment of the donor and acceptor molecules, to get physically relevant results, the value of κ^2 has to be estimated from the angle between the donor emission and acceptor absorption dipoles [14]. $J(\lambda)$, the overlap integral, which expresses the degree of spectral overlap between the donor emission and the acceptor absorption, is given by,

$$J(\lambda) = \frac{\int_0^\infty F_D(\lambda)\varepsilon_A(\lambda)\lambda^4\, d\lambda}{\int_0^\infty F_D(\lambda) d\lambda} \tag{4}$$

where $F_D(\lambda)$ is the fluorescence intensity of the donor in the wavelength range of λ to $\lambda + d\lambda$ and is dimensionless. $\varepsilon_A(\lambda)$ is the extinction coefficient (in $\mathrm{M}^{-1}\,\mathrm{cm}^{-1}$) of the acceptor at λ. If λ is in nm, then $J(\lambda)$ is in units of $\mathrm{M}^{-1}\,\mathrm{cm}^{-1}\,\mathrm{nm}^4$.

Once the value of R_0 is known, the efficiency of energy transfer can be calculated. The efficiency of energy transfer (E) is the fraction of photons absorbed by the donor which are transferred to the acceptor and is defined as,

$$E = \frac{k_T(r)}{\tau_D^{-1} + k_T(r)} \tag{5}$$

or

$$E = \frac{R_0^6}{r^6 + R_0^6}. \tag{6}$$

The transfer efficiency is measured using the relative fluorescence intensity of the donor, in absence (F_D) and presence (F_{DA}) of the acceptor as,

$$E = 1 - \frac{F_{DA}}{F_D}. \tag{7}$$

For D-A systems decaying with multiexponential lifetimes, E is calculated from the amplitude weighted lifetimes $\langle\tau\rangle = \sum_i \alpha_i\tau_i$ of the donor in absence (τ_D) and presence (τ_{DA}) of the acceptor as,

$$E = 1 - \frac{\tau_{DA}}{\tau_D}. \tag{8}$$

The D-A distances can be measured using equations (6)–(8). The distances measured using equations (7) and (8) are revealed as R^S (steady-state measurement) and R^{TR} (time-resolved measurement), respectively. In one of recent studies from our group [18], we have shown that the energy transfer efficiency E, calculated from steady-state experiment might be due to re-absorption of donor emission, but not due to dipole-dipole interaction (FRET).

2.2 Nanosurface energy transfer technique (NSET)

The D-A separations can also be calculated using another prevailing technique, NSET [19,20], in which the energy transfer efficiency depends on the inverse of fourth power of the donor-acceptor separation. Nano-surface energy transfer (NSET) technique is based on the model of Persson and Lang [21] which is concerned with the momentum and energy conservation in the dipole-induced formation of electron-hole pairs. Here the rate of energy transfer is calculated by performing a Fermi golden rule calculation for an excited-state molecule depopulating with the simultaneous scattering of an electron in the nearby metal to above the Fermi level. The Persson model states that the damping rate to a surface of a noble metal may be calculated by,

$$k_{et} = 0.3\left(\frac{\mu^2\omega_{dye}}{\hbar\omega_F k_F d^4}\right) \tag{9}$$

which can be expressed in more measurable parameters through the use of the Einstein A_{21} coefficient [22]

$$A_{21} = \frac{\omega_{dye}^3}{3\varepsilon_0\hbar\pi c^3}\left|\mu\right|^2. \tag{10}$$

To give the following rate of energy transfer, in accordance with Coulomb's law $(1/4\pi\varepsilon_0)$

$$k_{et} = 0.225\frac{c^3\Phi_{dye}}{\omega_{dye}^2\omega_F k_F d^4\tau_{dye}} \tag{11}$$

where c is the speed of light, Φ_{dye} is the quantum yield of the donor, ω_{dye} is the angular frequency for the donor, ω_F is the angular frequency for bulk metal, d is the donor-acceptor separation, τ_{dye} is the average lifetime of the dye and k_F is the Fermi wavevector for bulk metal. The d_0 value is a convenient value to calculate for a dye-metal system, yielding the distance at which a dye will display equal probabilities for energy transfer and spontaneous emission. For the Persson model, the d_0 value may be calculated by

$$d_0 = \left(0.225\frac{c^3\Phi_{dye}}{\omega_{dye}^2\omega_F k_F}\right)^{1/4}. \tag{12}$$

In our case, we have used the $k_{\text{time-resolved}}$ as k_{et},

$$k_{\text{time-resolved}} = \frac{1}{\tau_{\text{donor-acceptor}}} - \frac{1}{\tau_{dye}} \tag{13}$$

where $\tau_{\text{donor-acceptor}}$ is the average lifetime of the donor-acceptor system.

2.3 Lifetime and rotational relaxation measurement

Fluorescence transients were measured and fitted by using commercially available spectrophotometer (LifeSpec-ps) from Edinburgh Instrument, U.K (80 ps instrument response function (IRF)) with an attachment for temperature dependent studies (Julabo, Model F 32). The observed fluorescence transients are fitted by using a nonlinear least square fitting procedure to a function $(X(t) = \int_0^t E(t')R(t-t')dt')$ comprising of convolution of the IRF $(E(t))$ with a sum of exponentials $(R(t) = A + \sum_{i=1}^{N} B_i e^{-t/\tau_i})$ with pre-exponential factors (B_i), characteristic lifetimes (τ_i) and a background (A). Relative concentration in a multi-exponential decay is finally expressed as; $a_n = \frac{B_n}{\sum_{i=1}^{N} B_i}$. The average lifetime $(\langle\tau\rangle)$ is calculated as, $\langle\tau\rangle = \sum_i a_i\tau_i$.

For time resolved anisotropy measurements emission polarization is adjusted to be parallel and perpendicular to that of the excitation polarization and define anisotropy as,

$$r(t) = \frac{I_{para}(t) - GI_{perp}(t)}{I_{para}(t) + 2GI_{perp}(t)} \tag{14}$$

I_{para} and I_{perp} are detected emission intensities with polarization parallel and perpendicular respectively with respect to the excitation laser pulse. the magnitude of G, the grating factor of the emission monochromator of the TCSPC system was measured by following longtime tail matching technique [23].

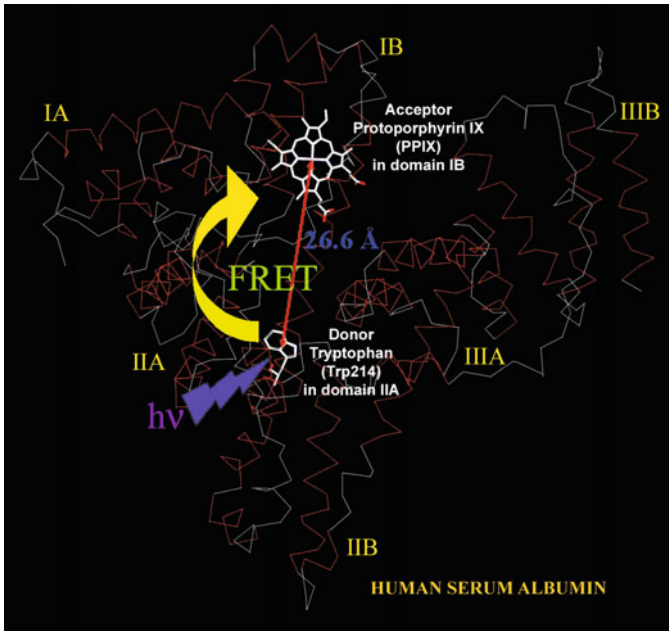

Fig. 2. (Color online) X-ray crystal structure of Human Serum Albumin depicting the FRET between the donor tryptophan (Trp214) and the acceptor Protoporphyrin IX (PPIX).
Reprinted from A.K. Shaw and S.K. Pal, J. Photochem. Photobiol. B Biol. **90**, 69 (2008). ©2008, with permission from Elsevier.

3 Results and discussions

3.1 Ultrafast resonance energy transfer in various folded states of a transporter protein human serum albumin (HSA) [11]

In this study, we have used one of the fluorescent amino acids, single Trp214 residue in HSA as a donor. The well known porphyrin, PPIX is used as model acceptor in the protein. Porphyrins belong to a class of tetrapyrroles having extensive applications as photosensitizers in medicine. Porphyrins are spectroscopically well characterized [24] and are known to serve as models for artificial solar energy capture as in photosynthesis. Crystallographic study [25] reveals that PPIX, a member of porphyrin family, binds to domain-IB of HSA (Fig. 2). Figure 3a shows the spectral overlap of emission spectra of the donor (Trp214 in domain-IIA of HSA) and the absorption spectrum of acceptor (PPIX in domain-IB of HSA) to N-form (native form) of HSA. A significant overlap indicative of considerable non-radiative transfer of excited state energy from Trp214 to PPIX is observed. This is also evident from quenching of fluorescence of Trp214 as revealed from steady-state fluorescence spectra (Fig. 3b) and faster decay of Trp214 fluorescence (Fig. 3c) in presence of PPIX. The average fluorescence lifetimes of Trp214 of HSA in presence and absence of PPIX are tabulated in Table 1. The calculated values of $J(\lambda)$, E, R_0 and the D-A separation (R) are tabulated in Table 1 for different conformations of HSA.

The X-ray crystal structure of methemalbumin indicates that there is definite geometric arrangement of

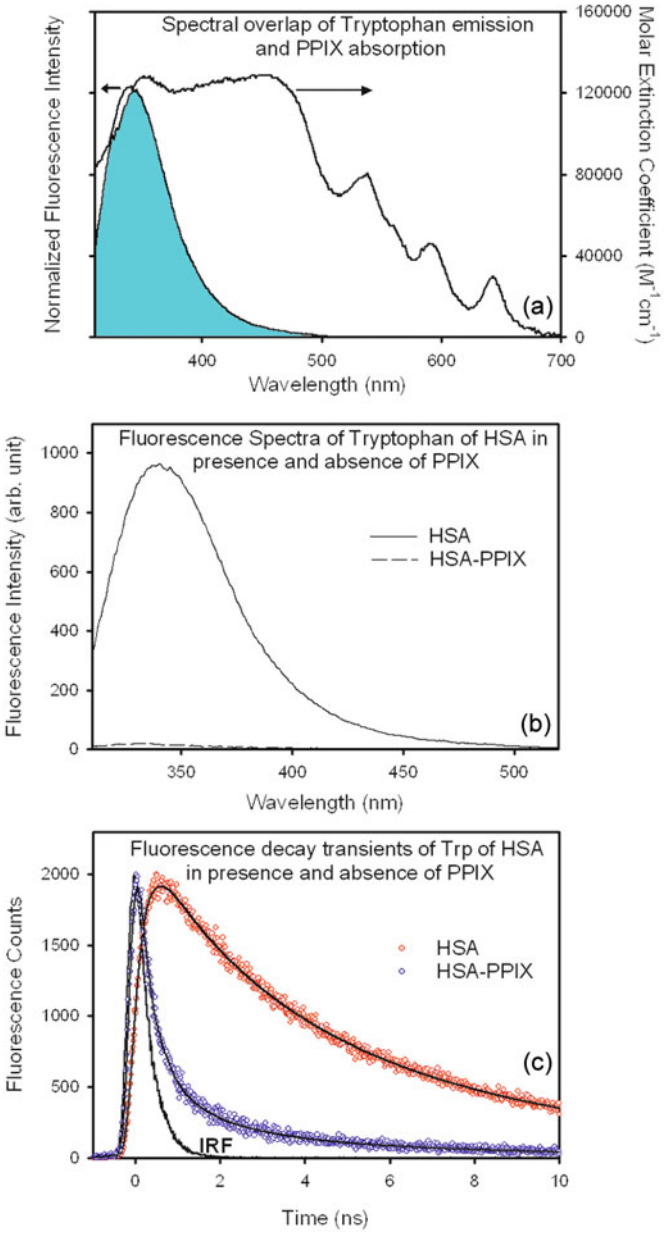

Fig. 3. (Color online) (a) Spectral overlap of fluorescence spectrum of Trp214 and absorption spectrum of PPIX bound to HSA at pH = 7, (b) fluorescence spectra (excitation = 297 nm) and (c) fluorescence decay transients of Trp214 (excitation = 299 nm, emission = 360 nm) in presence and absence of PPIX bound to HSA at pH = 7.

Haem605 and Trp214, thus κ^2 cannot be taken to be 0.67. In this case, we have calculated the κ^2 value of 0.9853 using equation (3) from the crystal structure of methemalbumin [25] and used the same for calculation of D-A separation. The D-A separation of 25.4 Å obtained for N-form HSA at 25 °C is in close agreement with the distance (26.6 Å) between Trp214 and Haem605 obtained from X-ray crystallographic study of PPIX bound to HSA [25]. At pH = 2 for extended form (E-form) HSA, the D-A separation of 33.9 Å is larger than that of N-form which is consistent with the increase in inter-domain separation and subsequent disruption of domain-I at 25 °C. Thus, significant loss of tertiary structure is observed at pH = 2. Upon increasing the temperature, the separation decreases to 17.0 Å in N-form HSA indicating closer approach of Trp214 and PPIX. This may be due to disruption of domain-II of HSA due to which Trp214 becomes a bit flexible and moves closer to PPIX in domain-I. Again at 75 °C, a slight increase in D-A separation to 18.6 Å may indicate the parting away of donor and acceptor due to disruption of domain-I above 60 °C. For E-form HSA at pH = 2, however there is a decrease in D-A separation from 25 °C till 75 °C. This may be due to the fact that in this acid-induced unfolded HSA where domain-II was in molten globule state starts unfolding with increase in temperature due to which D-A separation decreases leading to proximity of donor and acceptor. Further increasing the temperature to 75 °C causes the conformation to change in such a way that there occurs a further reduction in D-A separation. However, the aged form (A-form) HSA at pH = 11 shows almost no change in D-A separation. This may be due to the fact that HSA attains greater stability in alkaline solution compared to neutral and acidic pH solutions. Through this study the non-covalently bound PPIX is shown to be an efficient FRET probe in reporting the different temperature-induced folded states of HSA in buffer solutions of widely differing pH values.

3.2 Resonance energy transfer in synthetic and genomic DNA: importance of relative orientation of donor and acceptor in FRET [14]

The dynamics of FRET in synthetic dodecamer duplex DNA and genomic (from salmorn sperm) has been explored by using Hoechst 33258 (H258) and ethidium bromide (EtBr) as model donor and acceptor respectively. The donor ligand H258 is a well known minor groove binder [26]. The efficiency of EtBr as a DNA intercalator is also been recognized in the literature [27]. In a control experiment, we studied the resonance energy transfer between the ligands H258 (donor) and EtBr (acceptor) in sodium dodecyl sulfate (SDS) micelles. In the micellar system the D and A molecules can be bound simultaneously without any restriction on the relative orientation of their transition dipole moments. Thus the orientation parameter κ^2 can be taken as 0.667 [16] in the micellar system. The estimated distance between the D and A has been estimated to be 3.02 nm which is consistent with the binding of the D and A across the chord in the spherical SDS micelle (∼4 nm diameter).

However in the case of DNA, κ^2 should not be assumed to be 0.667 because of the specific binding geometry. Figure 4a shows the spectral overlap between absorption and emission spectrum of the EtBr (A) and H258 (D) respectively in 100 μM salmon sperm DNA. The concentration of the EtBr (10 μM) has been so chosen so as to assure

Table 1. Calculated values of parameters obtained from FRET between Trp214 (domain-IIA) and PPIX (domain-IB) to different conformers of HSA at different temperatures.

pH	Temperature (°C)	Peak (nm)	$\langle\tau_D\rangle$ (ns)	$\langle\tau_{DA}\rangle$ (ns)	$J(\lambda)$ $M^{-1}\,cm^{-1}\,nm^4$	E	R_0 (Å)	r (Å)
2	25	332	2.58	1.05	1.92×10^{15}	0.593	36.1	33.9
	60	334	0.99	0.50	1.87×10^{15}	0.495	30.7	30.8
	75	343	0.64	0.08	1.86×10^{15}	0.876	28.0	20.2
7	25	337	3.91	0.29	1.96×10^{15}	0.926	38.7	25.4
	60	332	1.96	0.03	1.69×10^{15}	0.984	33.9	17.0
	75	332	1.20	0.05	1.64×10^{15}	0.958	31.4	18.6
11	25	335	1.57	0.35	1.86×10^{15}	0.777	33.0	26.8
	60	331	0.38	0.11	1.75×10^{15}	0.697	33.1	28.8
	75	333	0.26	0.11	1.55×10^{15}	0.585	30.2	28.5

Reprinted from A.K. Shaw and S.K. Pal, J. Photochem. Photobiol. B Biol. **90**, 69 (2008). ©2008, with permission from Elsevier.

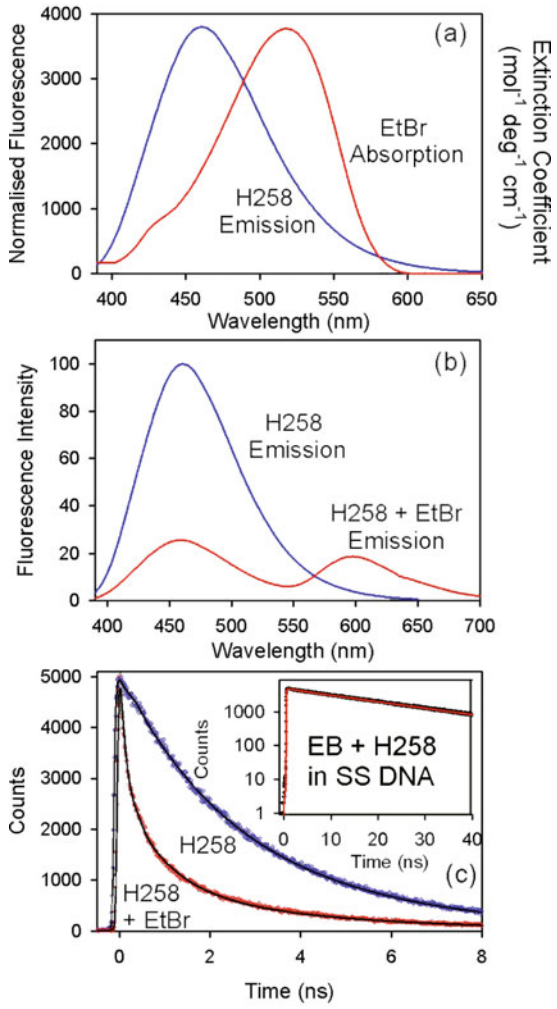

Fig. 4. (Color online) (a) The spectral overlap of H258 and EtBr in 100 mM (base pair) genomic DNA. The emission spectrum (b) and the temporal decay (c) of H258 (1 mM) and H258-EtBr ([EtBr] = 10 mM) in genomic DNA.

Reprinted with permission from D. Banerjee, S.K. Pal, J. Phys. Chem. B **111**, 5047 (2007). ©2007, American Chemical Society.

maximum intercalation of the dye (considering one ethidium molecule intercalates per 10 base pairs [28]). On the addition of acceptor (EtBr) molecules to H258-DNA solution, there is no shift in the emission maxima of the probe H258 compared to that of the H258-DNA complex without EtBr, indicating that the donor is still bound to the DNA. The binding of the ethidium molecules to DNA is confirmed by the 22 ns component in the temporal fluorescence decay characterizing the DNA environment [28] (inset of Fig. 4c). The quenching of the fluorescence intensity (Fig. 4b) coupled with the appearance of faster components in the decay (Fig. 4c) of the H258 in the presence of EtBr in the DNA suggests considerable energy transfer from the donor to the acceptor molecule. It has been suggested in a previous study [29] that the donor and the acceptor molecules in the genomic DNA cannot assume random orientations with respect to each other [29]. So the value of κ^2, which takes into account the relative orientation of the donor and acceptor transition dipoles [16], cannot be taken as 0.667, the value in the random orientation condition. In accordance with the above-mentioned study, the calculated value of R_0, using κ^2 value of 1.2 is found to be 3.23 nm. Analyses of the temporal decay curves along with the above mentioned D-A distances it is estimated that the centers of the H258 and EtBr molecules are separated by 5, 7 and 10 base pairs respectively within the persistence length of the genomic DNA. The D-A distance of 3.30 nm can also be assigned to donor and acceptors coming in close proximity due to folding and loop formation in genomic DNA [30]. So this study does not conclude that the donor and acceptor molecules are bound to the same region of the genomic DNA.

In order to verify whether the intercalator EtBr and groove binder H258 can bind to the same region of the DNA, the FRET studies are carried out in the dodecamer DNA. Each of the dyes individually binds to the dodecamer as shown in separate studies [28,31]. The X-ray crystal structure of H258 bound to the minor groove of the dodecamer shows that the probe binds to the central A-T rich sequence involving five base pairs [31]. In a solution containing both the dyes H258 and EtBr in dodecamer

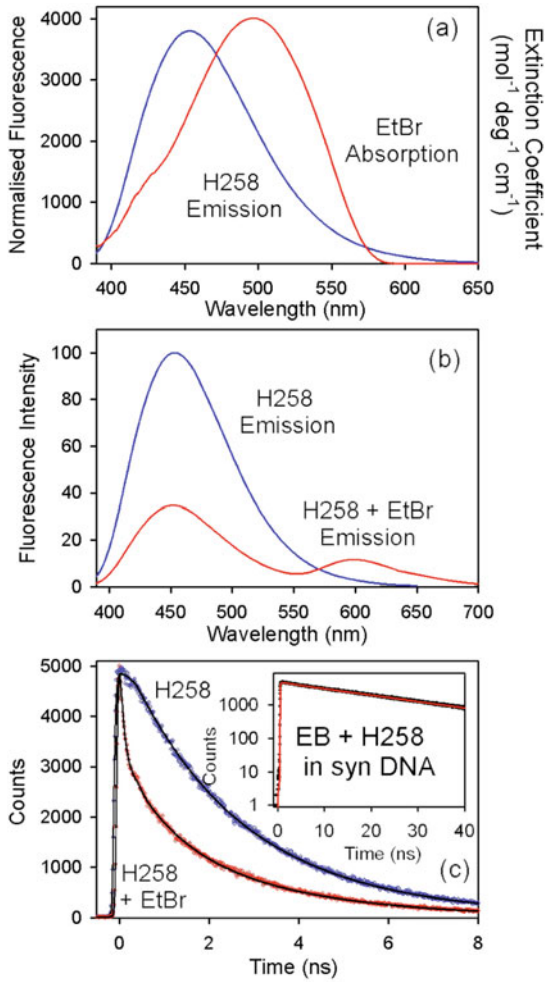

Fig. 5. (Color online) (a) The spectral overlap of H258 and EtBr in 70 mM (basepair) synthesized DNA ([DNA] = 5.8 mM). The emission spectrum (b) and the temporal decay (c) of H258 (1 mM) and H258-EtBr ([EtBr] = 6 mM) in synthesized DNA.

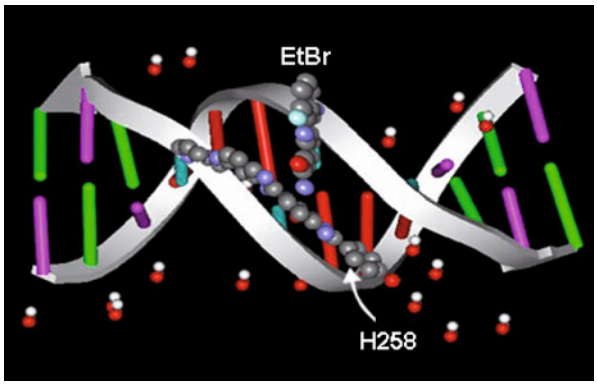

Fig. 6. (Color online) The transition dipoles of the donor (H258, minor groove binder)-acceptor (EtBr, intercalator) make an angle of 66° with respect to each other when bound to a single dodecamer.

DNA, the dye H258 shows emission maxima at 460 nm characteristic of minor groove binding (Fig. 5b), whereas the dye EtBr shows the 22 ns component at 620 nm indicative of intercalation (inset of Fig. 5c). Figure 5a, shows the spectral overlap between the emission spectra of the donor and the absorption spectra of the acceptor in the dodecamer. The quenching of fluorescence intensity (Fig. 5b) along with the faster temporal decay (Fig. 5c) in the H258-EtBr complex relative to that of the H258 in the dodecamer suggests energy transfer between the two molecules. To confirm that the energy transfer takes place between the dye-molecules bound to a single dodecamer, a control experiment is performed. As a control, two separate solutions, one containing the donor (H258) bound to dodecamer DNA and another containing acceptor (EtBr) bound to dodecamer DNA are mixed. The temporal decay of the resultant solution shows no faster component associated with energy transfer. The result confirms that the energy transfer is indeed intra-DNA. In the synthesized DNA, the molecules H258 and EtBr attain a definite geometry relative to each other. The transition dipole moment of EtBr is inclined 75° with respect to the helix axis [27,32,33]. The transition dipole of the minor groove-binding drug, H258 is perpendicular to the long axis of the minor groove, which in turn makes an angle of 51° with the helix axis. The transition dipoles of the D-A pair thus make an angle of 66° with respect to each other (Fig. 6). Using these results, the value of κ^2 was estimated to be 0.04 by using equation (3) and the R_0 value was calculated to be 1.91 nm. Thus consideration of the random orientation of the transition dipoles of the DA ($\kappa^2 = 0.667$) is expected to report erroneous result in the case of DNA.

3.3 Nonspecific protein-DNA interactions probed by FRET [34]

After the successful application of FRET in the case of isolated protein [11] and DNA [14] molecule, we were interested to apply the technique to explore interaction of protein with a genomic DNA (from salmon sperm). The protein is in the class of digestive enzyme of mammalian family called α-chymotrypsin (CHT), isolated from bovine pancreas and has biological function of hydrolyzing polypeptide chains. Here we used CHT bound ANS and DNA bound EtBr as model D-A system respectively. An extensive fluorescence study [35] followed by an X-ray study [36] on the ANS-CHT complex indicated that ANS binds rigidly at a single site on the surface of the protein near the Cys-1-122 disulfide bond. This ANS binding site is almost diametrically opposite in position to the enzymatic center. In Figure 7a, we present the steady-state fluorescence spectra of CHT-bound ANS and its complex with DNA. The emission intensity of ANS-CHT is observed to be similar to that of ANS-CHT-DNA complex revealing the fact that ANS molecules are not detached from CHT upon complexation. The time-resolved studies (Fig. 7b) also confirm the above results. The time-resolved anisotropy decay (at 480 nm) of ANS-CHT, shown in Figure 7c, revealed a rotational time constant of 47 ns,

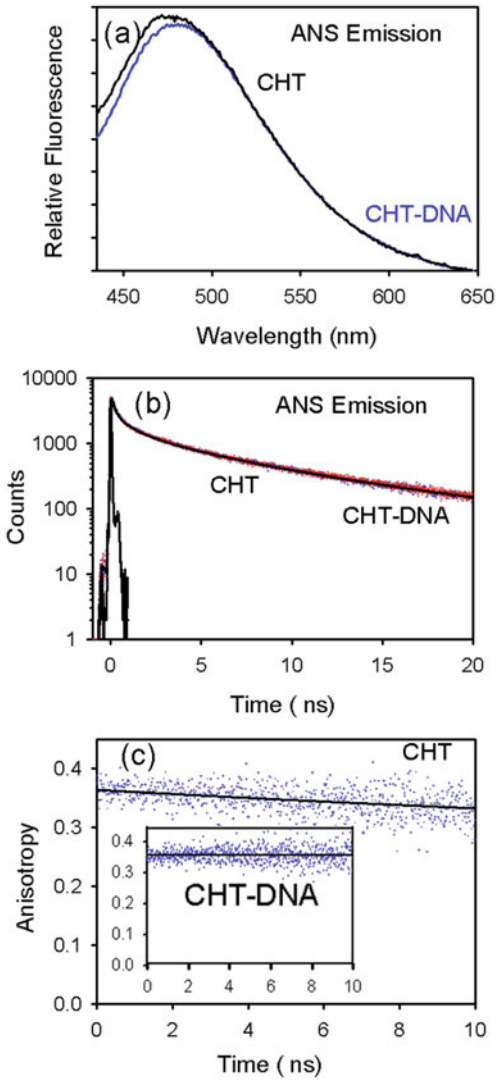

Fig. 7. (Color online) (a) Steady state fluorescence spectra of ANS bound to CHT in the presence and absence of SS DNA. (b) Time-resolved transients of ANS bound to CHT in the presence and absence of SS DNA. (c) Time-resolved anisotropy of ANS bound to CHT in the absence of the DNA. Inset shows the time-resolved anisotropy of ANS bound to CHT in presence of the DNA.

Reprinted with permission from S.S. Narayanan, S.K. Pal, Langmuir **23**, 6712 (2007). ©2007, American Chemical Society.

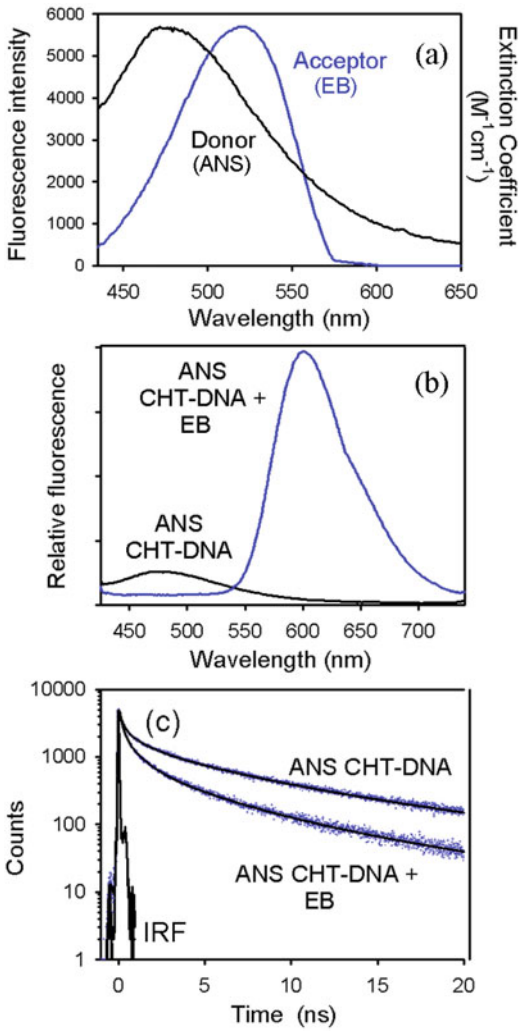

Fig. 8. (Color online) (a) Spectral overlap between donor (ANS-CHT-DNA complex) emission and acceptor (ANS-CHT with EB-bound DNA) absorbance. (b) Steady state fluorescence quenching of donor (ANS-CHT-DNA complex) in the presence of the acceptor ethidium bromide (EB) in the DNA. (c) Picosecond-resolved transients of donor (ANS-CHT-DNA complex) in the absence and presence of acceptor (EB) in the DNA.

Reprinted with permission from S.S. Narayanan, S.K. Pal, Langmuir **23**, 6712 (2007). ©2007, American Chemical Society.

attributed to the global tumbling motion of the protein CHT (see Ref. [34] for details). On the other hand the $r(t)$ decay of ANS-CHT-DNA complex (inset of Fig. 7c) exhibited a very long time component with a significantly large residual anisotropy (residual $r(t)$), which do not decay within our experimental time window. The above results confirm the rigidity of ANS-CHT complex and the suppression of CHT motion in the CHT-DNA complex.

The spectral overlap of the donor (ANS-CHT-DNA complex) emission and the acceptor (ANS-CHT with EB-labeled DNA) absorption spectra is shown in Figure 8a. As clearly evident from steady state fluorescence spectrum (Fig. 8b), the emission intensity of the donor is quenched on inclusion of acceptor (EB) in the DNA. The time-resolved studies also confirm the energy transfer process (Fig. 8c). The picosecond-resolved transient (Fig. 8c) of the donor reveals an average decay time constant of 0.88 ns as compared to 0.54 ns for the donor in the presence of the acceptor. The drop in the average decay time of donor-acceptor complex compared to that of the donor alone, also confirms that the energy transfer occurs from ANS to EB due to dipolar coupling. The calculated (from Eqs. (7) and (8)) donor to acceptor energy transfer efficiency from steady state and time-resolved studies are 39.6% and 34.1% respectively. The estimated D-A distances from steady state and time-resolved experiments

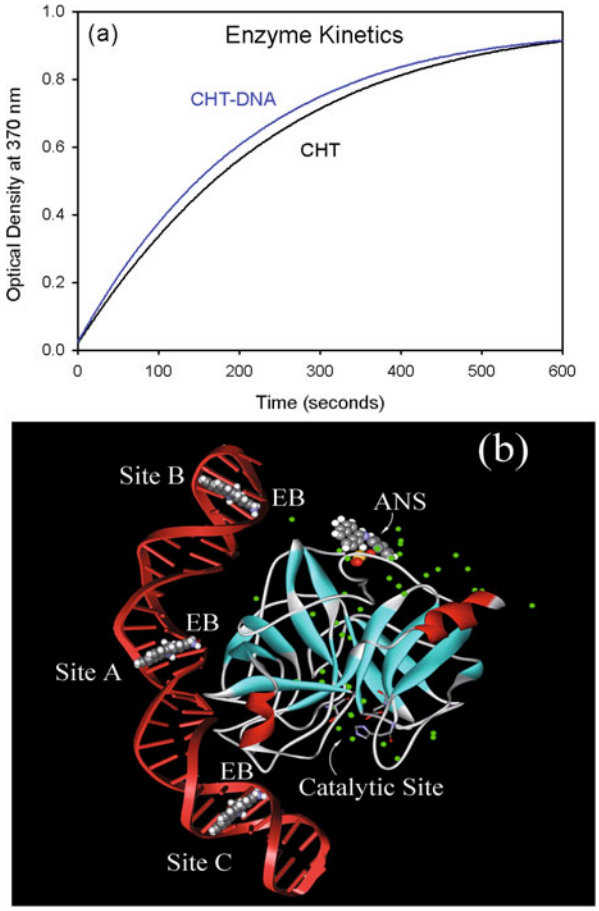

Fig. 9. (Color online) (a) Enzymatic activity of CHT on the substrate, AAF-AMC in the presence and absence of SS DNA. (b) The schematic representation of nonspecific protein-DNA binding interactions. The spheres indicate the water molecules observed in X-ray crystallographic study on the enzyme CHT. Reprinted with permission from S.S. Narayanan, S.K. Pal, Langmuir **23**, 6712 (2007). ©2007, American Chemical Society.

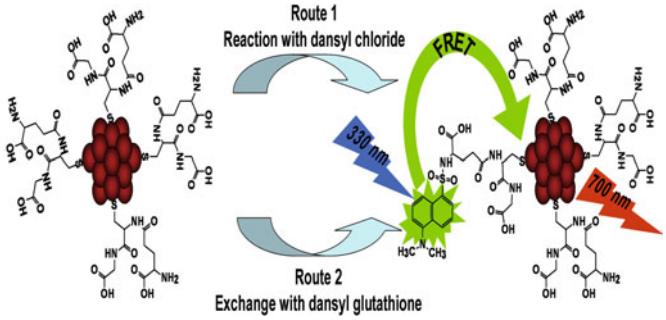

Fig. 10. (Color online) Approaches used for the functionalization of dansyl chromophore on the Au_{25} cluster. Reprinted with permission from M.A.H. Muhammed, A.K. Shaw, S.K. Pal, T. Pradeep, J. Phys. Chem. C **112**, 14324 (2008). ©2008, American Chemical Society.

are 22.9 Å and 23.8 Å, respectively. It should be noted that ANS binding site and the enzymatic active site of CHT are in almost diametrically opposite points [36]. The estimated distance between above two sites is ∼40 Å. Our measurement of ANS-EB distance of ∼23.5 Å reveals that the DNA interacts with CHT at a site, which is located between ANS-binding site and the enzymatic active site of CHT without perturbing the enzymatic property of the CHT (Fig. 9a). In the experiment we have maintained [DNA]:[EB] ratio in such a way that distance between two EB is expected to be 34 Å (10 bp) [37]. As shown in Figure 9b the measured ANS-EB distance (23.5 Å) could be average distance from ANS to EB at the site A and also at the site B. The energy transfer from ANS due to dipolar coupling to a distant EB at the site C is forbidden.

3.4 Quantum clusters of gold exhibiting FRET [38]

In this study, we explored the possibility of using gold nanoclusters of 25 atoms (Au_{25}) as energy acceptors in a FRET study. A dansyl chromophore is used as model donor molecule. Dansyl chromophore was attached to the Au_{25} core by two different routes. In the first route, dansyl chloride was reacted at the amino group of the glutamate residue of some of the glutathione ligands (-SG) anchored on Au_{25}. This gives Au_{25} cluster protected with a mixture of glutathione and N-dansyl glutathione. The product obtained in this route is referred to as the reaction product in the ongoing discussion. In the second route, some of the glutathione ligands of the cluster underwent exchange by the classical ligand exchange method with dansyl glutathione (-SG-D) when the $Au_{25}SG_{18}$ was stirred with dansyl glutathione. This method also led to the formation of Au_{25} protected with a mixture of glutathione and N-dansyl glutathione. The product obtained here is referred to as the exchange product (Fig. 10).

Steady state fluorescence measurements were carried out on both the exchange and reaction products in order to check whether any energy transfer occurred between the cluster and the chromophore. It was found that emission of dansyl glutathione underwent drastic quenching in both the products. Figure 11 depicts the emission profile of the reaction product. The quenching of the donor is seen clearly. On the other hand, the emission at 700 nm, which is the characteristic emission of Au_{25}, enhanced in both the reaction and the exchange products when excited at the excitation maximum of the donor (330 nm). It is clear from Figure 11 that the intensity of emission collected when excited at 535 nm (excitation maximum for the parent Au_{25}) is low when compared with the emission collected at 330 nm excitation. This clearly establishes energy transfer from the dansyl chromophore to Au_{25}.

From the femtosecond-resolved lifetime measurements, a faster decay of fluorescence is observed in both the dansylated products compared to the parent donor (Fig. 12). The decay is faster for the exchange product than the reaction product. Note that the chromophore underwent complete quenching in the case of exchange product and hence faster decay. From multiexponential fitting of the fluorescence transient of the donor, time constants of

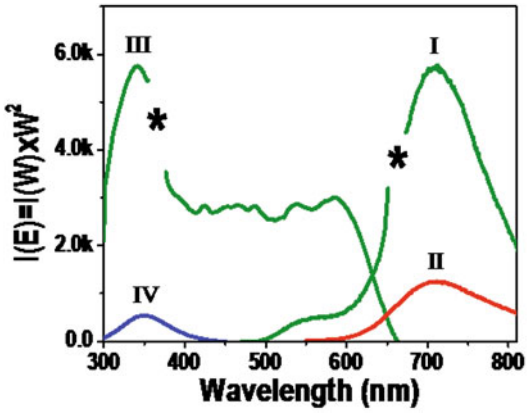

Fig. 11. (Color online) Steady state fluorescence spectra of the reaction product. (I) and (II) are the emission spectra obtained when excited at 330 and 535 nm, respectively showing the same emission maximum. Corresponding excitation spectra for emission at 700 and 550 nm are in (III) and (IV). The emission at 550 nm is the quenched donor emission. Asterisks correspond to regions where higher order lines of the grating mask the spectrum.

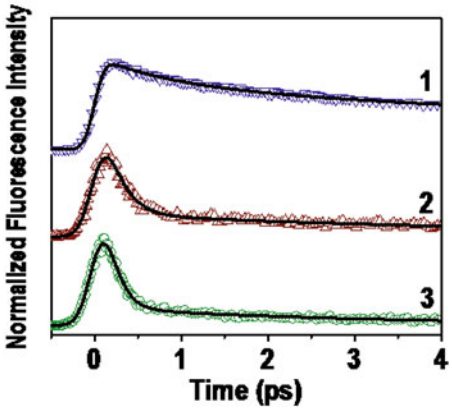

Fig. 12. (Color online) Femtosecond time-resolved fluorescence transients of (1) D-GSH, (2) reaction and (3) exchange products. The samples were excited at 364 nm and the transients were collected at 500 nm.

0.85 ps (29.6%), 6.40 ps (42.9%) and 39.05 ps (27.5%) are obtained. The time constants are consistent with the reported study on the ultrafast deactivation pathways of the dansyl fluorophore in bulk methanol. The femtosecond resolved study on the dansyl chromophore reveals that the sub-picosecond component is due to the ultrafast solvation dynamics in polar environments (water in our case) and other two components are associated with the structural relaxation of the probe. The excited state lifetime of the probe, which is reported to be 9–12 ns is reflected in the offset in the fluorescence decay, does not decay reasonably in our experimental window of 4 ps. The overall average lifetime of the probe of 13.75 ps is also consistent with the previous report. However, in case of the D-A systems, much shorter components of 0.20 ps (86.8%) and 5.10 ps (13.2%) for the reaction product and 0.15 ps (92.4%) and 3.00 ps (7.6%) for the exchange product are observed. The overall lifetimes of the probe in presence of acceptor Au_{25} (0.85 ps for reaction product and 0.35 ps for exchange product) reveal significant fluorescence quenching compared to that in donor (13.75 ps). This indicates that large non-radiative resonance energy transfer has taken place from the dansyl chromophore to Au_{25}. Since the percentage of dansyl glutathione per cluster is only 25, they are expected to be far apart due to steric effects and hence the dipole-dipole coupling within D-D pairs would be negligible.

Firstly we analyzed the energy transfer by FRET. The $J(\lambda)$ and R_0 are determined to be 1.91×10^{15} $M^{-1}\,cm^{-1}\,nm^4$ and 41 Å, respectively. The D-A separations (r) for the reaction and exchange products are 25.9 Å and 22.2 Å, respectively. This corresponds to a very high efficiency of energy transfer. The theoretically estimated distance between the Au_{25} cluster and the dansyl chromophore (centre to centre), assuming standard bond lengths is around 23 Å which matches with the experimental data. The D-A separations can also be calculated using another prevailing technique NSET. The calculated D-A values using NSET are 19.9 Å and 15.8 Å for the reaction and exchange products, respectively. In either case, the shorter D-A separation for exchange product is because during exchange, some of the glutathione ligands attached to the cluster are removed and dansyl glutathione occupies the space provided, with dansyl group projecting towards the liquid phase. In the reaction product, dansylation is carried out directly on the assembly of glutathione ligands on the cluster surface. Due to steric hindrance, reaction occurs only on those ligands which are farthest from the core and hence therefore a longer D-A distance. In either case, the data reflect the asymmetry in the ligand binding on the metal core, supporting the structures proposed using experiment and theory.

3.5 Ultrafast migration of electronic energy from a semiconductor quantum dot to a chemotherapeutic drug [39]

The suitability of a core/shell type CdSe/ZnS semiconductor QD as energy donor in FRET experiment has been investigated. A chemotherapeutic drug, Merocyanin 540 (MC540) attached to the surface of the QD is used as model energy acceptor. Figure 13a illustrates the absorption spectrum of QDs in toluene together with the spectral overlap between the emission spectrum of QDs and the absorption spectrum of the MC540 in toluene. MC540, an anionic cyanine dye, is a heterocyclic chromophore that is commonly used as a sensitizer in chemotherapy, and more recently as a sensitizer in photoelectrochemical cells for solar energy conversion [40]. The huge spectral overlap suggests that an efficient FRET between the donor

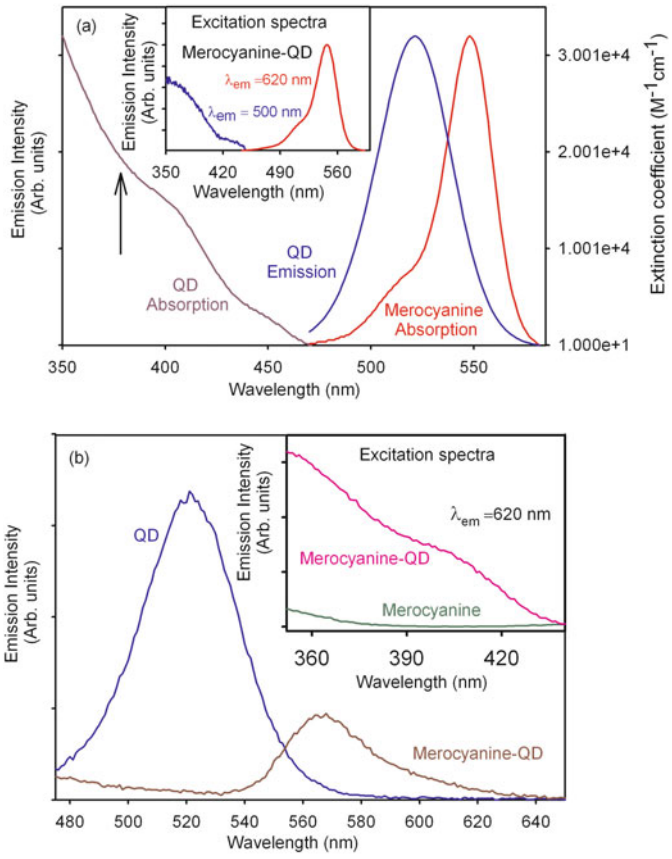

Fig. 13. (Color online) (a) Steady-state absorption spectrum of CdSe/ZnS core-shell QDs together with the spectral overlap between emission spectrum of QDs and the absorption spectrum of MC540. The inset shows the excitation spectra of QD-MC540 conjugate at $\lambda_{em} = 500$ and 620 nm. The arrow indicates the excitation wavelength (375 nm) used to excite QDs. (b) 375 nm laser light is used for the exclusive excitation of QDs in the conjugates, and the observed peak at 570 nm corresponding to the MC540 emission occurs as a result of FRET from the QDs. Inset shows the excitation spectra of MC540 and QD-MC540 conjugate at $\lambda_{em} = 620$ nm.

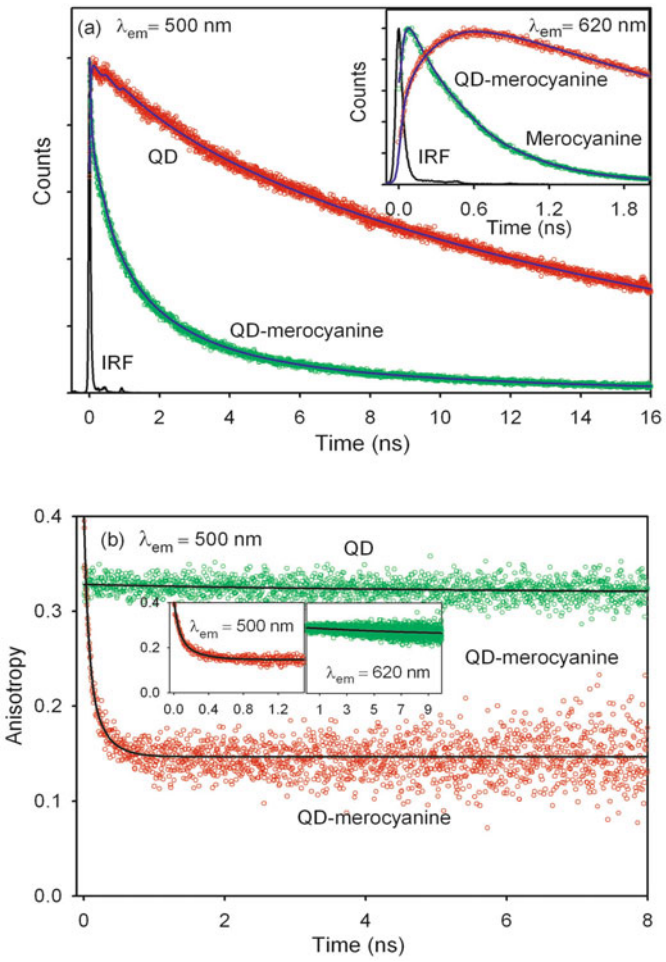

Fig. 14. (Color online) (a) Picosecond-resolved PL transients (instrument response function, IRF = 80 ps) of QD in the absence and presence of MC540 at $\lambda_{em} = 500$ nm. The inset shows the picosecond-resolved PL transients of MC540 and QD-MC540 conjugate at $\lambda_{em} = 620$ nm, clearly revealing a rise component for the QD-MC540 which is completely absent in the transient of MC540 alone. (b) Picosecond-resolved PL anisotropy of QD and QD-MC540 at $\lambda_{em} = 500$ nm. The inset shows the picosecond-resolved PL anisotropy of QD-MC540 at $\lambda_{em} = 500$ nm (left) in a time-window of 1.5 ns and at $\lambda_{em} = 620$ nm (right) in a time-window of 10 ns.

(QDs) and the acceptor (MC540) can take place when MC540 binds to the surface of QDs. For the energy transfer studies, the broad absorption spectrum of the QDs (Fig. 13a) enabled us to find a suitable wavelength where the donor QDs could be selectively excited without the acceptor drug getting appreciably excited. The arrow in the absorption spectrum of QDs in Figure 13a indicates the excitation wavelength used to excite QDs (i.e. 375 nm). It has to be noted that the excitation spectra of QD-MC540 complex at the emission peak of QDs (500 nm) and MC540 (620 nm) matches with their corresponding absorption spectra (inset of Fig. 13a) indicating negligible perturbation in the spectroscopic properties of either QDs or MC540 in the QD-MC540 complex.

It has been reported that FRET can be an efficient process between QDs and dyes, including photosensitizers [41]. Figure 13b reveals a significant quenching in the steady-state PL intensity of the QDs (emission peak 520 nm) in the QD-drug complex on exciting at 375 nm. This was accompanied by an increase in the fluorescence of MC540 (emission peak 570 nm) as a result of FRET. These observations are confirmed by fluorescence lifetime measurements, where a substantial shortening of the QD donor lifetime is measured in the presence of the drug (Fig. 14a). However, the quenching observed here could be due to either energy transfer or other non-radiative processes [42] between QDs and the drug molecules. This is easily verified by monitoring the lifetime components of QD-MC540 at the emission peak of acceptor. As shown

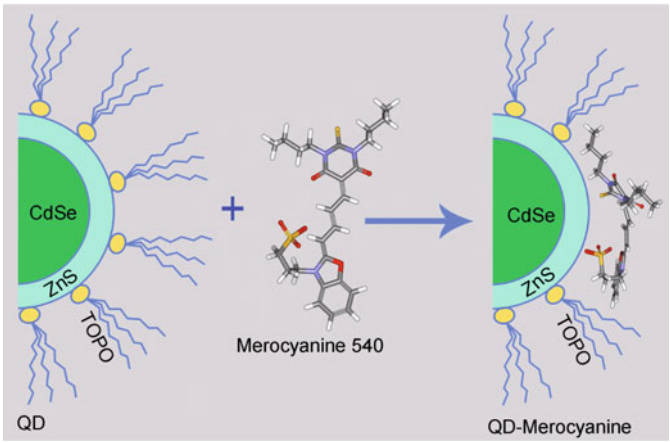

Fig. 15. (Color online) Binding of drug molecules (MC540) to the surface of CdSe/ZnS QDs due to strong affinity of sulfur atom of MC540 compared to the oxygen atom of the TOPO on the surface of QDs.

in the inset of Figure 14a, QD-MC540 at 620 nm shows a clear signature of a rise component of 254 ps, indicating a significant energy transfer from QDs to the drug via FRET. It is expected that the QD emission at 520 nm is transferred non-radiatively to MC540 through space dipole-dipole coupling leading to detection of sensitized emission from the drug at 570 nm. The signature of the sensitized emission from the drug is also borne out from the excitation spectrum of QD-MC540 monitored at 620 nm (inset of Fig. 13b). Upon monitoring emission of QD-MC540 at 620 nm, which solely originates from the MC540 emission, the excitation spectrum is found to be identical with the absorption profile of the free QDs (inset of Fig. 13b). No such signature is found in the excitation spectrum of MC540 alone clearly indicating the sensitized emission from acceptor.

The picosecond-resolved transients of QDs (donor) alone at $\lambda_{em} = 500$ nm reveals multiexponential decay [43] with an average time constant of 12 ns compared to 0.6 ns for the conjugate system. This gives a FRET efficiency of 95% and a donor-acceptor distance of 25 Å. This is consistent with the report by Tsay et al. [44] concerning the FRET studies between peptide-coated green-emitting QDs and rose bengal where they reported a drastic shortening of the fluorescence lifetime of QDs upon conjugation to rose bengal. Moreover, the FRET efficiency obtained by them (>90%) closely matches with our results (95%). It is known that the diameter of the CdS core is 21 Å and the thickness of shell is around 3 Å (provided by Evident technologies). Also, the size of the TOPO molecule around the QD is 12 Å. Taken together, the radius of the TOPO-capped core-shell QD will be ∼26 Å. The estimated D-A distance of ∼26 Å in QD-MC540 complex clearly supports our model of direct binding of drug molecule to the surface of CdSe/ZnS QDs, making the FRET process efficient (Fig. 15).

We have further probed the QD-MC540 system by undertaking the time-resolved anisotropy measurements. Figure 14b shows the picosecond-resolved PL anisotropy decays of QDs and QD-MC540 at 500 nm. QDs in toluene (500 nm) reveal anisotropy decay with a rotational time constant of 8 ns. On the other hand, QD-MC540 revealed a major contribution of fast component of 130 ps together with a minor contribution of a slow component of 8 ns. The observation of a higher contribution of fast component (130 ps) in the conjugate indicates the exciton migration in the QDs which transfers its energy to the proximal drug molecules through dipole-dipole coupling leading to a strong sensitized emission from the drug. Using the time-resolved fluorescence anisotropy study, Ghiggino and coworkers [45] have demonstrated the dynamics of energy transfer in multiporphyrin functionalized dendrimers where they observed a fast decay in the anisotropy profile before leveling off to a non-zero residual anisotropy similar to our observation. They explained their observation to the ability of these molecules to absorb light and then efficiently delocalize the excitation energy over the chromophore arrays during the energy migration process. The left inset of Figure 14b shows picosecond-resolved anisotropy decay of QD-MC540 in a small time-window. The anisotropy decay of QD-MC540 at 620 nm (right inset of Fig. 14b) reveals a very slow component which does not decay within our experimental window, characteristic of drug bound to QDs. Using the hydrodynamic diameter, we also calculated the rotational correlation time (τ_r) of QDs using the Stokes Einstein Debye (SED) theory and found a value of 9.5 ns, close to the experimentally obtained value and consistent with our report on a similar system [46]. The observation of fast decay component in the anisotropy of QD-MC540 complex in contrast with the slow decay component in the anisotropy of QD alone provides strong evidence that FRET occurs between QDs and drug molecules.

3.6 Ultrafast resonance energy transfer to a molecular magnet confined in the nanocage of a globular protein in various folded states [12]

Recently a new class of magnetic materials, called molecular magnets, has attracted much attention due to their unusual properties that in general are associated with mesoscopic magnetism and quantum effects. Among these, polyoxovanadate $[V_{15}As_6O_{42}(H_2O)]^{-6}$ clusters (denoted as V_{15}) shows the essential properties of a single molecule magnet. Due to a huge overlap of the optical absorption spectrum of V_{15} with the emission spectrum of a fluorescence center of HSA (from the single Trp214) there is a possibility of energy transfer by radiationless dipole-dipole coupling (Fig. 16). Figure 17a indeed reveals a huge overlap of the emission spectrum of HSA with the absorption spectrum of V_{15}. The resulting energy transfer leads to an efficient modification of the fluorescence dynamics of the Trp214 in HSA and therefore the emission of HSA suffers a huge quenching upon complexation with V_{15} (Fig. 17b). To have a better insight on the observed quenching, we

Table 2. Time resolved fluorescence decay and FRET data of the Trp214 residue in HSA at different temperatures in absence and presence of V_{15}.

Temperature (K)	τ_1 (ps)	τ_2 (ps)	τ_3 (ps)	$\langle\tau_D\rangle$ (ps)	$\langle\tau_{DA}\rangle$ (ps)	E	$J(\lambda)\times10^{13}$	r (Å)
HSA in water								
293	880 (0.15)	5850 (0.85)	–	5090	–	–	–	–
303	1370 (0.30)	5850 (0.70)	–	4500	–	–	–	–
313	830 (0.26)	4900 (0.74)	–	3820	–	–	–	–
323	800 (0.30)	4350 (0.70)	–	3280	–	–	–	–
333	1030 (0.42)	4050 (0.58)	–	2780	–	–	–	–
HSA + V_{15}								
293	20 (0.64)	440 (0.18)	2090 (0.18)	–	470	0.91	9.03	16.0
303	50 (0.51)	790 (0.29)	2280 (0.20)	–	710	0.84	9.00	17.5
313	80 (0.44)	1030 (0.41)	3270 (0.15)	–	950	0.75	9.00	19.0
323	100 (0.42)	1040 (0.37)	4020 (0.21)	–	1290	0.60	8.97	21.5
333	340 (0.29)	1500 (0.37)	4170 (0.34)	–	2070	0.25	8.97	28.0

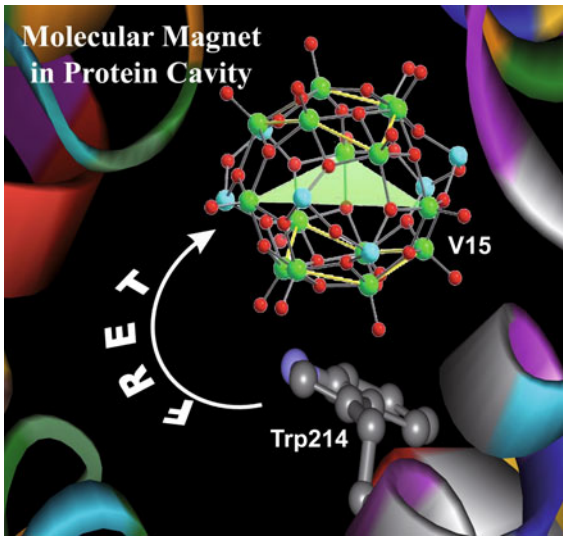

Fig. 16. (Color online) A molecular magnet V_{15} in ball-and-stick representations of the cluster anion (V = green; As = light blue, O = red) emphasizing the central V_3 triangle (transparent green), is shown in a hydrophobic cavity of a human serum albumin (HSA). The proximity of the single tryptophan (Trp214) is also shown.

perform time-resolved fluorescence measurements of the systems (Figs. 17c–17d, Tab. 2). The decay transient of HSA at 293 K can be fitted bi-exponentially with time constants of 880 ps (15%) and 5850 ps (85%), with an average lifetime ($\langle\tau_D\rangle$) of 5090 ps (Tab. 2). In presence of V_{15} the decay is dominated by a fast component and could only be fitted tri-exponentially with time constants of 20 ps (64%), 440 ps (18%) and 2090 ps (18%), with the average lifetime of the HSA-V_{15} conjugate $\langle\tau_{DA}\rangle$ = 470 ps. This indicates a quenching of fluorescence by more than an order of magnitude. As the temperature is increased, $\langle\tau_D\rangle$ of HSA decreases steadily and at 333 K, it becomes half of the value at 293 K (Tab. 2). However, in presence of V_{15}, $\langle\tau_{DA}\rangle$ increases steadily leading to a value five times larger at 333 K compared to that at 293 K (Tab. 2). Such a reversal of the temperature effect is quite unusual. We attribute the fast component (of the order of tens of ps), that is present in the conjugate and absent in HSA, to the quenching of the fluorophore upon addition of V_{15}. With increase in temperature this component gets gradually slower and signifies the release of quenching, similar to the steady state measurements (Fig. 17b).

From the average lifetime $\langle\tau_D\rangle$ of the donor (HSA), $\langle\tau_{DA}\rangle$ of the conjugate (HSA+V_{15}) and the extent of the overlap between the emission spectrum of HSA and absorption spectrum of V_{15}, the distance between Trp and V_{15} can be determined. The distances calculated at different temperatures (Tab. 2) are well within the range of the inter-domain distance of the protein [47]. This further supports the interaction between the entrapped V_{15} and Trp [48].

3.7 Resonance energy transfer from an intrinsic fluorescent amino acid Trp214 to a covalently attached semiconductor quantum dot in a transporter protein [13]

The efficiency of the intrinsic Trp214 in the globular transporter protein HSA as energy donor in FRET experiments has already been established in previous studies. Hence we concentrated on the dynamics of the FRET of Trp214 to a covalently attached cadmium sulfide (CdS) semiconductor QDs. The covalent binding of CdS to HSA

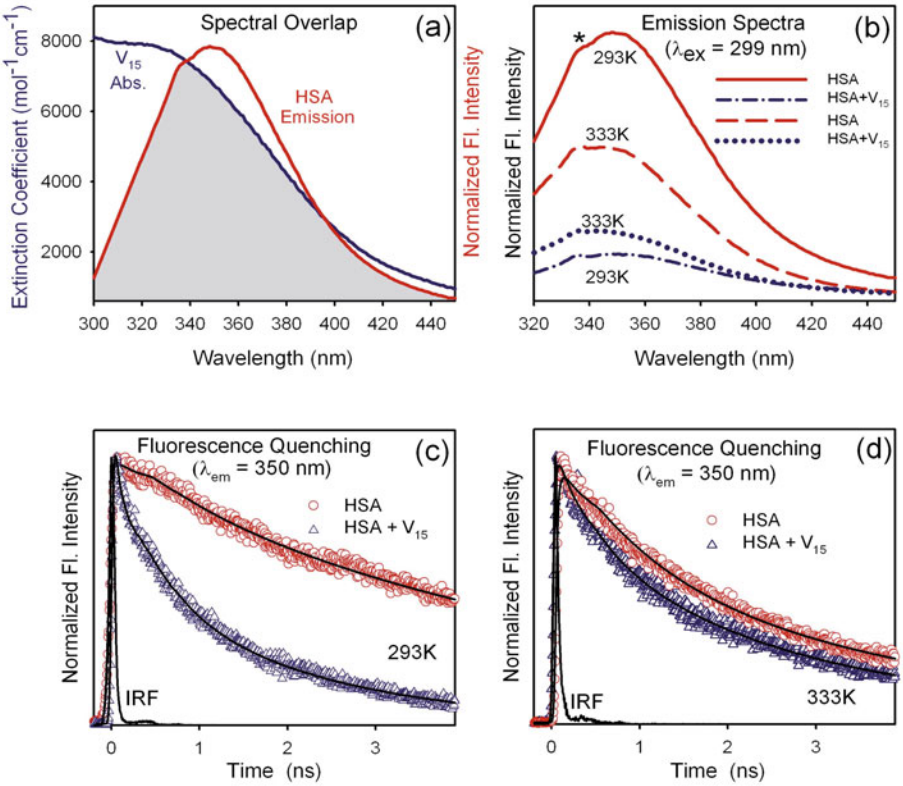

Fig. 17. (Color online) (a) Absorption and emission spectra of V_{15} and HSA in aqueous solutions. The shaded region is the area of overlap between the two spectra. This area is a measure of the distance between the donor (Trp residue of HSA) and V_{15} (see text for details). (b) Effect of temperature on the emission spectrum of HSA in absence and presence of V_{15}. The marker * stands for a Raman signal. (c), (d) Time resolved fluorescence decay of Trp residue in HSA measured at 350 nm in absence and presence of V_{15} at 293 K (c) and 333 K (d). The solid lines are bi (or tri) exponential decay fitted curves.

From Chem. Phys. Chem. **11**, 389 (2009). Copyright Wiley-VCH Verlag GmbH & Co. KGaA. Reproduced with permission.

Table 3. Helix-content, picosecond-resolved transients and energy transfer parameters of HSA before and after labeling with CdS nanocrystal. Here Q_D, R_0 and r denote quantum yield of the donor in absence of the acceptor, Förster distance and D-A distance respectively.

Systems	Temperature	α-helix content (%)	τ_1 in ns (%)	τ_2 in ns (%)	τ_3 in ns (%)	Q_D	R_0 (Å)	r (Å)
HSA	25 °C	69.7	0.23 (18.1)	1.65 (23.6)	5.99 (58.3)			
	60 °C	58.4	0.15 (29.4)	1.46 (31.3)	4.56 (39.3)			
	75 °C	45.9	0.11 (40.8)	1.15 (32.6)	3.82 (26.6)			
	60 °C (reverse)	49.4	0.09 (45.5)	1.08 (30.3)	3.69 (24.2)			
	25 °C (reverse)	60.5	0.13 (36.7)	1.23 (30.0)	4.63 (33.3)			
HSA-CdS	25 °C	76.4	0.08 (73.8)	1.45 (16.6)	5.99 (9.6)	0.097	32.1	26.1
	60 °C	66.9	0.08 (72.4)	1.12 (20.6)	4.56 (7.0)	0.092	32.9	27.7
	75 °C	58.8	0.07 (69.8)	0.92 (24.0)	3.82 (6.2)	0.087	31.6	28.6
	60 °C (reverse)	55.2	0.06 (72.9)	0.89 (20.0)	3.69 (7.1)	0.091	33.0	30.4
	25 °C (reverse)	60.4	0.05 (75.9)	1.02 (15.3)	4.63 (8.8)	0.091	33.0	28.8

Reprinted with permission from R. Sarkar, S.S. Narayanan, L.-O. Pålsson, F. Dias, A. Monkman, S.K. Pal, J. Phys. Chem. B **111**, 12294 (2007). ©2007, American Chemical Society.

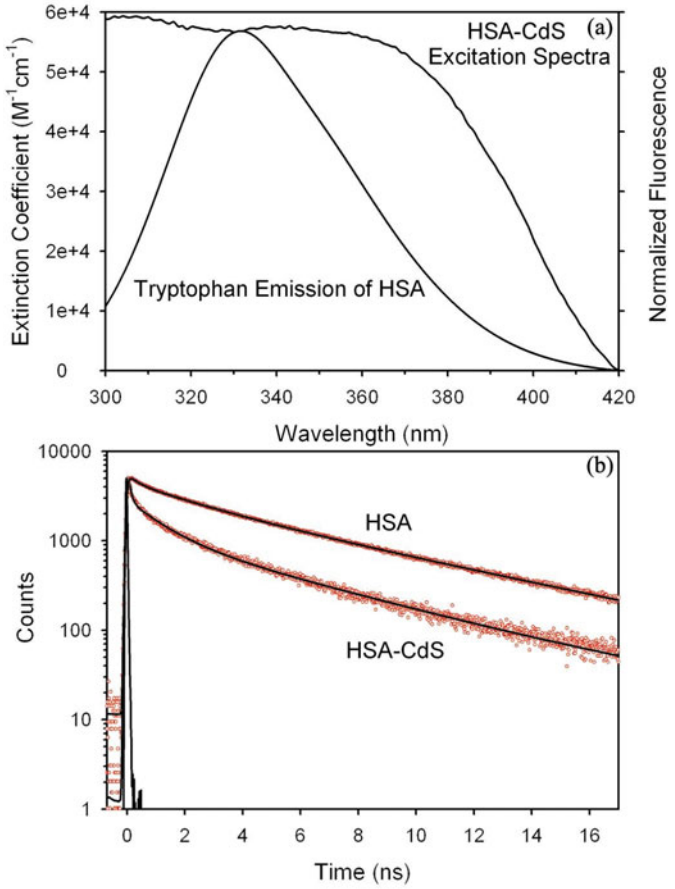

Fig. 18. (Color online) (a) Spectral overlap between the donor (tryptophan in HSA, Trp214) emission and acceptor (CdS tagged with HSA) excitation. (b) Picosecond-resolved fluorescence transients of Trp214 in HSA (excitation wavelength 299 nm and detection wavelength 360 nm) in absence and presence of CdS quantum dots in aqueous solution.

Reprinted with permission from R. Sarkar, S.S. Narayanan, L.-O. Pålsson, F. Dias, A. Monkman, S.K. Pal, J. Phys. Chem. B **111**, 12294 (2007). ©2007, American Chemical Society.

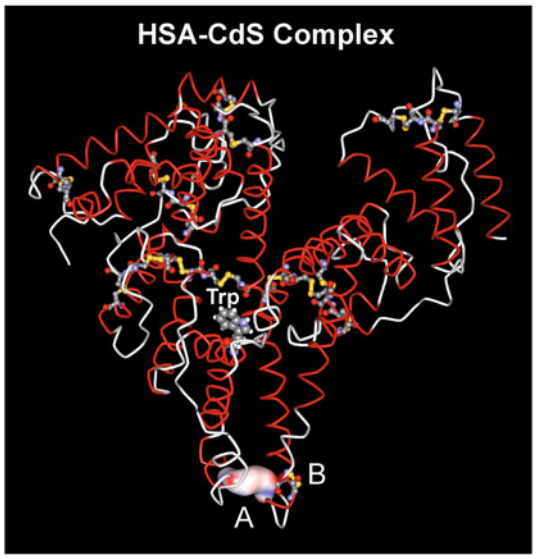

Fig. 19. (Color online) Three dimensional structure of HSA is presented. The location of Tryptophan 214 (Trp) is indicated. The possible sites for CdS attachment, site A and site B essentially indicate the positions of the Cys316-Cys361 and Cys360-Cys369 disulfide bonds respectively. Nucleation of the nanocrystal is likely to occur in the site A (see text). The solvent accessible surface area (SASA) of site A is also shown. Ball-stick models are used to indicate other disulfide bonds of the protein. The coordinates of HSA structure is downloaded from protein data bank (PDB code 1UOR) and processed with WebLab Viewer Lite program.

Reprinted with permission from R. Sarkar, S.S. Narayanan, L.-O. Pålsson, F. Dias, A. Monkman, S.K. Pal, J. Phys. Chem. B **111**, 12294 (2007). ©2007, American Chemical Society.

is confirmed by Matrix assisted laser desorption ionization (MALDI)-mass spectrometry analysis (data not shown here). Figure 18a shows the spectral overlap of the tryptophan emission (D, emission maximum at 332 nm) and CdS excitation (A, excitation spectrum maximum at 370 nm) in HSA at room temperature. The quenching of donor emission is evident from the faster lifetime (excitation source = 299 nm) associated with donor-acceptor pair (HSA labeled with CdS nanocrystal) compared to that in the donor alone (unlabeled HSA) (Fig. 18b, Tab. 3). The D-A distances (r) obtained from FRET experiments with varying temperature are summarized in Table 3. The average D-A distance at room temperature is found to be 26.1 Å. The measured distance indicates that the possible locations of CdS are close to either Cys316-Cys361 (distance from Trp214 = 27.4 Å) or Cys360-Cys369 (distance from Trp214 = 27.5 Å) which are in subdomain IIB and significantly exposed to the solvent environment [49], as indicated by A & B sites of (Fig. 19). We have further estimated solvent accessible surface area (SASA) of the two sites of HSA using WebLab viewer Lite program and found to have values 184.6 and 179.1 Å^2 respectively. Higher value of SASA of the site A compared to that of the site B makes the former site more favorable for CdS attachment. (See Ref. [13] for details.)

3.8 Silver (Ag) nanoclusters covalently conjugated to enzyme, CHT exhibiting resonance energy transfer [50]

In this study, we synthesized luminescent Ag nanocluster covalently attached to CHT at a site away from catalytic center of the enzyme. We demonstrated that nontoxic Ag nanoclusters could work as an efficient energy acceptor in FRET studies on biomolecules. Here we used NPA (NPA, a fluorescent probe is known to bind at the enzymatic active site [51]) as fluorescent energy donor. The huge overlap between NPA-CHT emission and the absorption of Ag-CHT nanocluster is expected to reveal inter-probe distance, when they are in a close proximity (Fig. 20). Figure 21a reveals the significant spectral overlap between NPA-CHT emission spectrum (D, emission maximum at 428 nm) and Ag-CHT excitation spectrum (A, excitation maximum at 413 nm) that favors the energy transfer from

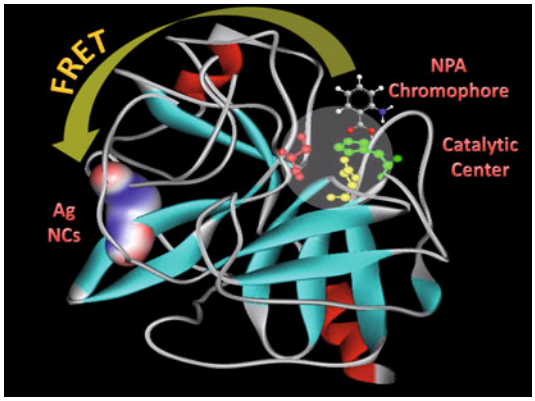

Fig. 20. (Color online) Structure of α-chymotrypsin depicting the catalytic triad (His57, Asp102 and Ser195), NPA chromophore binding site and luminescent Ag nanocluster (covalentely attached at a site away from catalytic center).

NPA to Ag in CHT. It has to be noted that the absorption band of Ag-CHT bioconjugates remained same even after the reconstitution process. As revealed from Figure 21b the overall steady-state emission intensity of the donor emission drastically decreased in the presence of acceptor. Also, the faster decay of donor in the presence of acceptor (Fig. 21c) as compared to that of the donor alone confirms the energy transfer from NPA to Ag cluster in CHT. The calculated (from Eqs. (7) and (8)) donor to acceptor energy transfer efficiency from steady-state and time-resolved studies are 97.5% and 60.7% respectively. The estimated donor-acceptor distances from steady-state and time-resolved experiments are 19.1 and 32.6 Å, respectively.

3.9 Ultrafast Förster energy transfer from 3-mercaptopropionic acid-capped CdSe/ZnS QDs to dye-labeled DNA [52]

Core-shell CdSe/ZnS QDs are probably the most successful type of QDs that have been developed and remained the best available for biological applications. Out of a variety of techniques developed, heterobifunctional ligands such as thiol-alkyl acids have been one of the most commonly used surface chemistries for the water solubility and bioconjugation of CdSe/ZnS QDs. The major advantage of using thiol-alkyl acid surface chemistry lies in the fact that these short-chain mercapto-carbonic ligands provide a very compact water solubilizing shell around the CdSe/ZnS QDs. Hence, these QDs are highly suited for FRET based studies and applications. Inset of Figure 22a illustrates the absorption and emission spectra of MPA-capped CdSe/ZnS QDs in buffer after the ligand-exchange procedure. It indicates that the QDs retained their photoluminescence properties when transferred into water using the literature procedure, which is important for fully harnessing the superior qualities of these fluorescent nanocrystals for applications in aqueous media. The direct bonding of MPA ligands onto the QD surface ensured that the overall size of the QDs remained small with

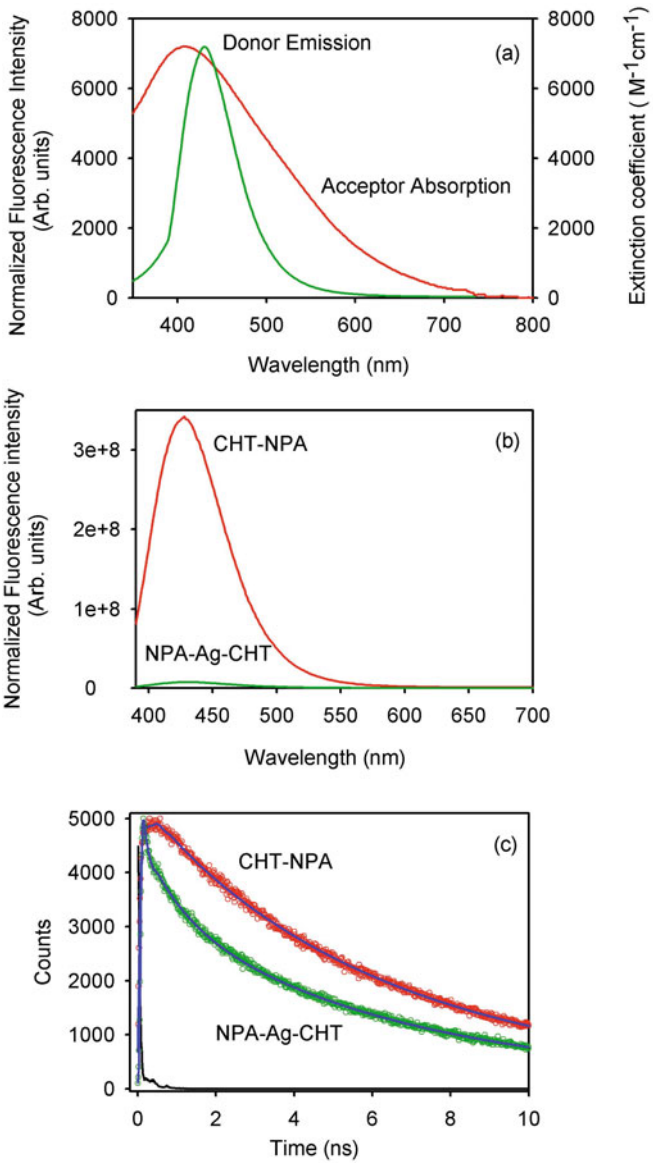

Fig. 21. (Color online) (a) Spectral overlap between the donor (NPA-CHT) emission and acceptor (Ag-CHT) absorption. (b) Steady-state photoluminescence quenching of NPA-CHT (donor) in the presence of acceptor (Ag-CHT nanobioconjugates). The optical density of the samples at excitation and emission wavelengths was 0.05 and 0.07, respectively. (c) Picosecond-resolved fluorescence transients of donor (NPA-CHT) and donor-acceptor (NPA-Ag-CHT) complex.

a thin solubilizing shell to increase the efficiency for energy transfer, which is important for FRET applications.

The inset of Figure 22a also reveals a huge spectral overlap between the emission spectrum of QDs and the absorption spectrum of EB-DNA (EtBr-DNA) complex suggesting that efficient FRET between the donor (QDs) and the acceptor (EB-labeled DNA) can take place when DNA is adsorbed onto the surface of QDs. We confirmed that only a slight overlap between the donor and acceptor

fluorescence occurred, allowing for the effective separation of donor fluorescence from that of the acceptor. Hence, we expect that the adsorption of EB-labeled-DNA onto the surface of MPA-capped QDs will result in the quenching of the QD fluorescence at 528 nm, while at the same time enhancing the EB fluorescence at 600 nm through FRET which was confirmed through both steady-state and time-resolved experiments as described below. Figure 22a shows the picosecond-resolved PL transients of QD and QD-(EB-DNA) conjugate at 528 nm. The picosecond decay of QDs in buffer revealed multiexponential [43] time constants of 0.31 ns (28%), 4.83 ns (26%) and 19.44 ns (46%) giving an average time constant ($\langle\tau\rangle$) of 10.3 ns. For the donor-acceptor system i.e. QD-(EB-DNA) complex, the time constants obtained were 64 ps (73%), 0.7 ns (14%), 3.85 ns (9%) and 11.54 ns (4%) revealing an average time constant ($\langle\tau\rangle$) of 0.92 ns. The substantial shortening in the QD exciton lifetime upon conjugate formation indicate conclusively that efficient FRET occurs from the QD donor to the EB-DNA acceptor. Based on the spectral overlap and using equation (8), we estimated a FRET efficiency of 92% in our FRET system. The Förster distance, R_0, for the QD-(EB-DNA) complex measured using equation (2) is 3.2 nm. In order to obtain the ultrafast component in the FRET system which was missing in our picosecond measurements due to its limited IRF, we performed femtosecond fluorescence upconversion measurements.

For CdSe/ZnS QDs (donor) in buffer, the upconverted fluorescence decay (Fig. 22b) revealed an ultrafast rise component of 430 fs together with a shorter decay component of 6 ps. The ultrafast rise time of 430 fs is attributed to the buildup of the lowest (1S) electron state in CdSe/ZnS QDs and is consistent with the femtosecond transient absorption measurements on colloidal CdSe QDs having a radius of 4.2 nm by Klimov and McBranch [53] where they reported a rise time of ∼400 fs. Using femtosecond fluorescence upconversion technique, Underwood et al. [54] reported a rise time of ∼530 fs for the 72 Å CdSe QDs compared to ∼270 fs for the 30 Å CdSe QDs. Energy relaxation following the optical excitation leads to the establishment of quasi-equilibrium populations of electron and hole quantized states. Depopulation of these states can occur via a variety of radiative and non-radiative mechanisms. The most important processes competing with the radiative ones are carrier trapping at surface/interface states. The short-lived component, representing the lifetime of fluorescence decay at the band edge, comprises both a radiative decay from electron-hole recombination and a non-radiative decay via trap states [55]. Because of the surface passivation of the core CdSe QDs with ZnS shell, the surface trapping process can be assumed to be negligible. Hence, the fast relaxation time constant of 6 ps could be assigned to the direct recombination of the exciton [56]. However, the contribution of surface states in the decay component of 6 ps cannot be completely ruled out due to the presence of MPA at the outer surface of QDs which has the ability to act as hole traps for these QDs [57]. We also obtained a slow decay component of 310 ps in the femtosecond measurement which was also confirmed in the picosecond-resolved experiment. Together with 310 ps, picosecond-resolved decays of QDs (Fig. 22a) in buffer also revealed time constants of 4.8 ns and 19.4 ns.

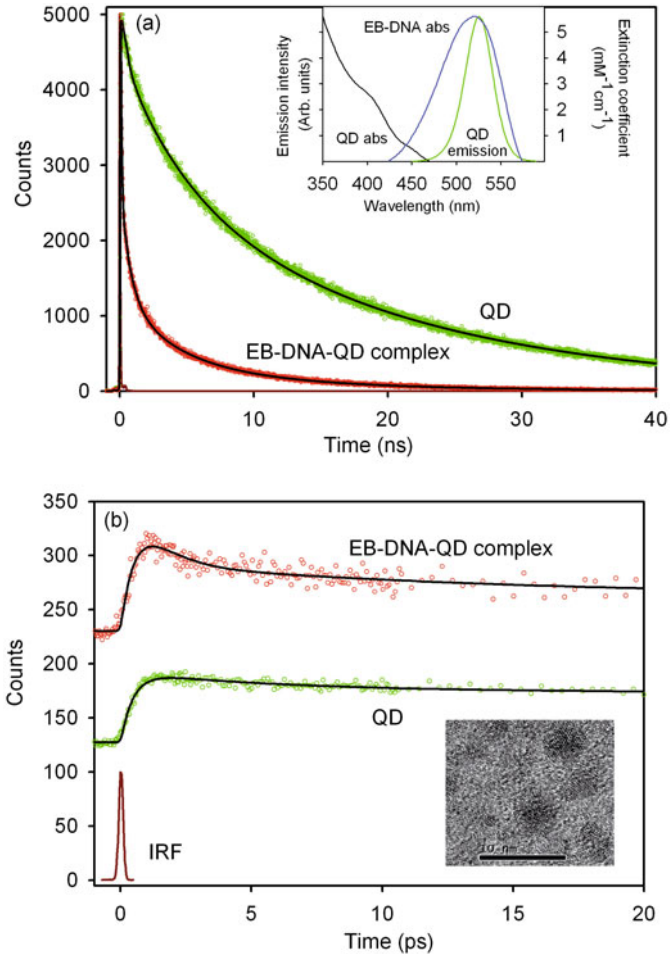

Fig. 22. (Color online) (a) Picosecond-resolved PL transients (instrument response function, IRF = 80 ps) of MPA-capped CdSe/ZnS QDs and (EB-DNA)-QD complex monitored at λ_{em} = 528 nm. Inset shows the steady-state absorption spectrum of MPA-capped CdSe/ZnS core-shell QDs in buffer together with the spectral overlap between emission spectrum of QDs and the absorption spectrum of EB-labeled DNA (the extinction coefficient value is for the acceptor, EB-labelled DNA). (b) Femtosecond-resolved fluorescence upconversion decay of MPA-capped CdSe/ZnS core-shell QDs and QD-(EB-DNA) complex monitored at λ_{em} = 528 nm. The dark red decay is the IRF (instrument response function) of the femtosecond pulse. Inset shows the HRTEM image of QD.

The picosecond-resolved decay time constants of donor and donor-acceptor systems together with their average time-constants ($\langle\tau\rangle$) have been listed in Table 4. The long-lived component of ∼10 ns could be assigned to the radiative recombination of the carriers bound to trap states [58] or due to the relaxation from a triplet state to the ground

Table 4. Fitted decay time constants of QD and QD-(EB-DNA) complex from picosecond and femtosecond experiments.

System	Picosecond experiment					Femtosecond experiment			
	τ_1 (α_1) (ns)	τ_2 (α_2) (ns)	τ_3 (α_3) (ns)	τ_4 (α_4) (ns)	$\langle\tau\rangle$ (ns)	τ_1 (α_1) (ps)	τ_2 (α_2) (ps)	τ_3 (α_3) (ps)	$\langle\tau\rangle$ (ps)
QD	0.31 (0.28)	4.83 (0.26)	19.44 (0.46)	–	10.3	5.9 (0.27)	634.2 (0.73)	–	466.4
QD-EB-DNA	0.064 (0.73)	0.7 (0.14)	3.85 (0.09)	11.54 (0.04)	0.92	0.93 (0.77)	13.3 (0.1)	269 (0.13)	36.4

Reprinted from S.S. Narayanan, S.S. Sinha, P.K. Verma, S.K. Pal, Chem. Phys. Lett. **463**, 160 (2008). ©2008, with permission from Elsevier.

state [54]. We have also measured the femtosecond dynamics of QD-(EB-DNA) complex (donor-acceptor system) and obtained a rise component of 640 fs, decay components of 935 fs and 13 ps, and a long component of 269 ps in the fitted decay (Fig. 22b). The faster decay time scales for the donor-acceptor system compared to donor alone conclusively indicates an efficient ultrafast energy transfer from the MPA-capped CdSe/ZnS QDs to the adsorbed EB-DNA complex. The femtosecond-resolved decay time constants of donor and donor-acceptor systems together with their average time-constants ($\langle\tau\rangle$) have been listed in Table 4. The FRET efficiency obtained from the femtosecond experiment was found to be 91% similar to that obtained from picosecond measurements (Fig. 23). It has to be mentioned that the percentage of donor QDs which contribute to FRET, specified by the percentage of the additional faster component in the time-resolved fluorescence decay of QD-(EB-DNA) complex (at 528 nm), which is absent in the donor fluorescence, has been estimated to be ∼75%. To confirm that the fluorescence quenching observed here is due to FRET only, a titration experiment with free DNA only (without intercalated EB) has been performed. We found negligible quenching of the QD emission with each aliquot of DNA added. Moreover, time-resolved decays of QD and QD-DNA were found to be almost overlapping each other. These studies clearly points out that the mechanism behind the quenching of QDs is only FRET.

It is known that the diameter of the CdSe core is 2.1 nm and the thickness of shell is approximately 1 nm (Evident Technologies). Also, the size of the MPA molecule is approximately 0.6 nm. Taken together, the radius of the MPA-capped CdSe/ZnS QD will be 2.6 nm. The estimated QD radius is in good agreement with the donor-acceptor distance of ∼2.5 nm from the center of the QD core to the surface of the QD where (EB-DNA) will bind, suggesting that DNA molecules are adsorbed onto the surface of QDs through the hydrogen-bonding interactions. Due to the small length of the DNA (12-merDNA) and hence its high flexibility, it is expected that the DNA molecules can adopt a conformation that lies along the surface of the MPA-capped QD analogous to the observation made for the adsorption of mixed base oligonucleotides on MAA-capped CdSe/ZnS QDs [59]. It has to be mentioned that the most probable location for the intercalation of EB to dodecamer DNA is between the central AT base pair. However, EB-intercalation on the GC sites can not be completely ruled out. Nevertheless, the difference in the distances in the two locations of EB in the dodecamer is expected to be negligibly small, considering the fact that the dodecamer interact length-wise with the QDs.

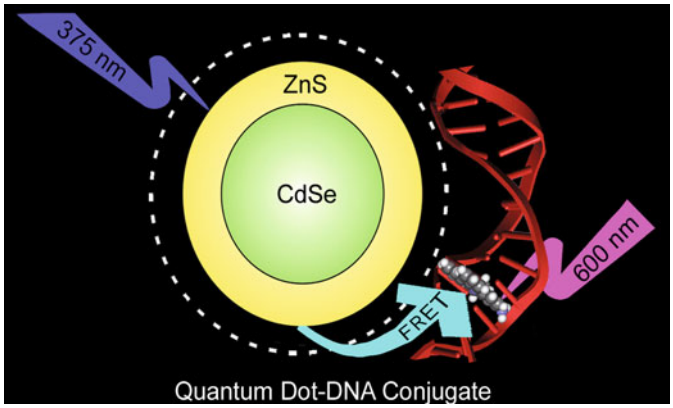

Fig. 23. (Color online) Study of ultrafast Förster resonance energy transfer from CdSe/ZnS QDs to ethidium bromide-labelled DNA using femtosecond and picosecond-resolved spectroscopic measurements.

Reprinted from S.S. Narayanan, S.S. Sinha, P.K. Verma, S.K. Pal, Chem. Phys. Lett. **463**, 160 (2008). ©2008, with permission from Elsevier.

4 Conclusion

The works covered by this review demonstrate the impressive array of experimental techniques that have been used to study FRET in simple biomimetic systems and then applied to more complex biological system. Our study on different conformers of HSA at different temperatures reflects the efficiency of a non-covalently bound probe, PPIX to act as an acceptor of non-radiative energy from intrinsic donor fluorophore (Trp214) present in domain-IIA of HSA for applying FRET technique. The reported studies on FRET between the dyes H258 and EtBr with simultaneous binding to dodecamer DNA, where the ligands have a particular relative orientation of the transition dipoles, in contrast to the cases in SDS micelles and larger genomic DNA, where the orientations are random, reveal the effect of the binding geometry of the ligands in the

constrained environment. Nonspecific protein-DNA interactions of a digestive protein CHT with genomic DNA have been probed by FRET. The non-radiative energy transfer from donor ANS (ANS-CHT-DNA complex) to the acceptor EtBr (ANS-CHT with EtBr labeled DNA) revealed that the protein-DNA complexation have minimal effect on the biological function of the protein.

The use of inorganic nanocrystals (QDs) in energy transfer by radiationless dipole-dipole coupling between donor and acceptor can be studied using two different models, namely FRET and NSET. Efficient energy transfer from dansyl chromophore (attached to Au_{25} cluster core through a tripeptide) to the Au_{25} core has established validation of FRET over NSET. We have investigated a FRET-based DA system in which the sensitized emission from the acceptor has been characterized by a fast component of the donor (QDs) fluorescence decay together with a corresponding rise component of similar time-scale for the acceptor (MC540). To the best of our knowledge, there are no reports which have shown the sensitized emission from a drug conjugated to QDs through a rise component at the emission peak of acceptor via time-resolved photoluminescence. Having characterized the importance of FRET between quantum clusters or quantum dot and tripeptide or drug we moved to real biological macromolecules. In this regard we have incorporated a molecular magnet (V_{15}) into a protein (HSA) cavity. This incorporation leads to FRET based on a spectral overlap between the excited state dipole (D) of the Trp in HSA with a dipole (A) in the molecular magnet. The resulting energy transfer leads to an efficient modification of the fluorescence dynamics of the Trp in HSA and therefore we can expect an efficient quenching of its emission spectrum as required in order to minimize the effect of UV damage on protein. Next to this incorporation we monitored FRET from the intrinsic fluorescent amino acids Trp214 of HSA (D) to CdS QDs (A) (here the semiconductor nanocrystals were covalently attached to the transporter protein). In continuation to this work, we have also synthesized luminescent Ag nanoclusters (1 nm average diameter) directly conjugated to an enzyme, CHT. In this case, we did not use intrinsic tryptophan rather labeled CHT at its enzymatic site by a fluorescent probe NPA and confirmed FRET between NPA bound at the enzymatic active site of CHT, as the donor and Ag nanoclusters-bound CHT as the acceptor. We did not limit ourselves to protein, we have also confirmed a highly efficient ultrafast FRET from MPA-capped CdSe/ZnS QDs to dye molecules attached to dodecamer DNA. The high FRET efficiency and the corresponding D-A distance of 2.5 nm suggest that adsorptive interactions between the DNA molecules and MPA-capped QDs result in a conformation that lies across the surface of the QD. These studies opens up a possibility that organic dyes as well as QDs can be used as a mediator that can couple its dipole with the excited state dipole of tryptophan (integral part of protein) or dye labeled protein/DNA to make a complete FRET system. This exploration on the ultrafast migration of resonance energy might be useful for the recovery of the damage through a directed resonance energy transfer in biologically relevant chromophores as well as light harvesting processes in biological systems.

P.K.V. thanks CSIR, India, for providing research fellowship. We thank DST, India, for financial grant (SR/SO/BB-15/2007). We thank colleagues in our laboratory at S.N. Bose whose contributions over the years, acknowledged in the references, have been instrumental in the successful evolution of work in this area. In particular, we thank Dr Rupa Sarkar, Dr. Ajay K. Shaw, M.A. Habeeb Muhammed, Dr. S. Shankara Narayanan, and Dr. Debapriya Banerjee. We thank Prof. T. Pradeep, IIT Madras (India) for the collaboration work.

References

1. J.-L. Ravanat, T. Douki, J. Cadet, J. Photochem. Photobiol. B: Biol. **63**, 88 (2001)
2. J.-M.L. Pecourt, J. Peon, B. Kohler, J. Am. Chem. Soc. **123**, 10370 (2001)
3. O.D. Schärer, Angew. Chem. **115**, 3052 (2003)
4. M.K. Cichon, S.A. Arnold, T. Carell, Angew. Chem. Int. Ed. **41**, 767 (2002)
5. J.D. Watson, F.H.C. Crick, Nature **171**, 964 (1953)
6. E. Chargaff, Science **172**, 637 (1971)
7. P.H. Clingen, C.F. Arlett, L. Roza, T. Mori, O. Nikaido, M.H.L. Green, Cancer Res. **55**, 2245 (1995)
8. A. Sancar, Chem. Rev. **103**, 2203 (2003)
9. A. Sancar, Biochemistry **33**, 2 (1994)
10. P.F. Heelis, R.F. Hartman, S.D. Rose, J. Photochem. Photobiol. A: Chem. **95**, 89 (1996)
11. A.K. Shaw, S.K. Pal, J. Photochem. Photobiol. B Biol. **90**, 69 (2008)
12. R.K. Mitra, P.K. Verma, D. Wulferding, D. Menzel, T. Mitra, A.M. Todea, P. Lemmens, A. Mueller, S.K. Pal, Chem. Phys. Chem. **11**, 389 (2010)
13. R. Sarkar, S.S. Narayanan, L.-O. Pålsson, F. Dias, A. Monkman, S.K. Pal, J. Phys. Chem. B **111**, 12294 (2007)
14. D. Banerjee, S.K. Pal, J. Phys. Chem. B **111**, 5047 (2007)
15. L. Stryer, Ann. Rev. Biochem. **47**, 819 (1978)
16. J.R. Lakowicz, *Principles of fluorescence spectroscopy* (Kluwer Academic/Plenum, New York, 1999)
17. S.E. Braslavsky, E. Fron, H.B. Rodríguez, E.S. Román, G.D. Scholes, G. Schweitzer, B. Valeur, J. Wirz, Photochem. Photobiol. Sci. **7**, 1444 (2008)
18. P. Majumder, R. Sarkar, A.K. Shaw, A. Chakraborty, S.K. Pal, J. Colloid Interface Sci. **290**, 462 (2005)
19. M. Montalti, N. Zaccheroni, L. Prodi, N. O'Reilly, S.L. James, J. Am. Chem. Soc. **129**, 2418 (2007)
20. S.-J. Chen, H.-T. Chang, Anal. Chem. **76**, 3727 (2004)
21. B.N.J. Persson, N.D. Lang, Phys. Rev. B **26**, 5409 (1982)
22. D. Craig, T. Thirunamachandra, *Molecular quantum Electrodynamics* (Academic Press, London, 1984)
23. D.V. O'Conner, D. Philips, *Time Correlated Single Photon Counting* (Academic Press, London, 1984)
24. N.C. Maiti, S. Mazumdar, N. Periasamy, J. Phys. Chem. **99**, 10708 (1995)
25. M. Wardell, Z. Wang, J.X. Ho, J. Robert, F. Florian Ruker, J. Ruble, D.C. Carter, Biochem. Biophys. Res. Comm. **291**, 813 (2002)

26. R. Jin, K.J. Breslauer, Proc. Natl. Acad. Sci. USA **85**, 8939 (1988)
27. D.P. Millar, R.J. Robbins, A.H. Zewail, Proc. Natl. Acad. Sci. USA **77**, 5593 (1980)
28. R. Sarkar, S.K. Pal, Biopolymers **83**, 675 (2006)
29. S. Murata, J. Kuśba, G. Piszczek, I. Gryczynski, J.R. Lakowicz, Biopolymers **57**, 306 (2000)
30. O.V. Tsodikov, R.M. Saecker, S.E. Melcher, M.M. Levandoski, D.E. Frank, M.W. Capp, M.T.J. Record, J. Mol. Biol. **294**, 639 (1999)
31. M.C. Vega, I.G. Saez, J. Aymami, R. Eritja, G.A.V. D. Marel, J.H. V. Boom, A. Rich M. Coll, Eur. J. Biochem. **222**, 721 (1994)
32. M. Tsuboi, J.M. Benevides, G.J.J. Thomas, Biophys. J. **92**, 928 (2007)
33. M. Levitt, Proc. Natl. Acad. Sci. USA **75**, 640 (1978)
34. S.S. Narayanan, S.K. Pal, Langmuir **23**, 6712 (2007)
35. J.D. Johnson, M.A. El-Bayoumi, L.D. Weber, A. Tulinsky, Biochemistry **18**, 1292 (1979)
36. L.D. Weber, A. Tulinsky, J.D. Johnson, M.A. El-Bayoumi, Biochem. **18**, 1297 (1979)
37. B. Saif, R.K. Mohr, C.J. Montrose, T.A. Litovitz, Biopolymers **31**, 1171 (1991)
38. M.A.H. Muhammed, A.K. Shaw, S.K. Pal, T. Pradeep, J. Phys. Chem. C **112**, 14324 (2008)
39. S.S. Narayanan, S.S. Sinha, S.K. Pal, J. Phys. Chem. C **112**, 12716 (2008)
40. F.M. Hamer, *The Chemistry of Heterocyclic Compound. The Cyanine Dyes and Related Compounds* (Interscience, New York, 1963)
41. A.C.S. Samia, X. Chen, B.C., J. Am. Chem. Soc. **125**, 15736 (2003)
42. C. Burda, X. Chen, R. Narayanan, M.A. El-Sayed, Chem. Rev. **105**, 1025 (2005)
43. M.G. Bawendi, P.J. Carroll, W.L. Wilson, L.E. Brus, J. Chem. Phys. **96**, 946 (1992)
44. J.M. Tsay, M. Trzoss, L. Shi, X. Kong, M. Selke, M.E. Jung, S. Weiss, J. Am. Chem. Soc. **129**, 6865 (2007)
45. E.K.L. Yeow, K.P. Ghiggino, J.N.H. Reek, M.J. Crossley, A.W. Bosman, A.P.H.J. Schenning, E.W. Meijer, J. Phys. Chem. B **104**, 2596 (2000)
46. S.S. Narayanan, R. Sarkar, S.S. Sinha, F. Dias, A. Monkman, S.K. Pal, J. Phys. Chem. C **112**, 3423 (2008)
47. S. Sugio, A. Kashima, S. Moshizuki, M. Noda, K. Kobayashi, Protein Eng. **12**, 439 (1999)
48. S.S. Sinha, R.K. Mitra, S.K. Pal, J. Phys. Chem. B **112**, 4884 (2008)
49. X.M. He, D.C. Carter, Nature **358**, 209 (1992)
50. S.S. Narayanan, S.K. Pal, J. Phys. Chem. C **112**, 4874 (2008)
51. R.P. Haugland, L. Stryer, in *Conformation of Biopolymers* (Academic press, New York, 1967)
52. S.S. Narayanan, S.S. Sinha, P.K. Verma, S.K. Pal, Chem. Phys. Lett. **463**, 160 (2008)
53. V.I. Klimov, D.W. McBranch, Phys. Rev. Lett. **80**, 4028 (1998)
54. D.F. Underwood, T. Kippeny, S.J. Rosenthal, J. Phys. Chem. B **105**, 436 (2001)
55. M.D. Garrett, M.J. Bowers, J.R. McBride, R.L. Orndorff, S.J. Pennycook, S.J. Rosenthal, J. Phys. Chem. C **112**, 436 (2008)
56. V.I. Klimov, J. Phys. Chem. B **104**, 6112 (2000)
57. S. Jeong, M. Achermann, J. Nanda, S. Ivanov, V.I. Klimov, J.A. Hollingsworth, J. Am. Chem. Soc. **127**, 10126 (2005)
58. T. Inokuma, T. Arai, Phys. Rev. B **42**, 11093 (1990)
59. W.R. Algar, U.J. Krull, Langmuir **22**, 11346 (2006)